

AD-A109 947

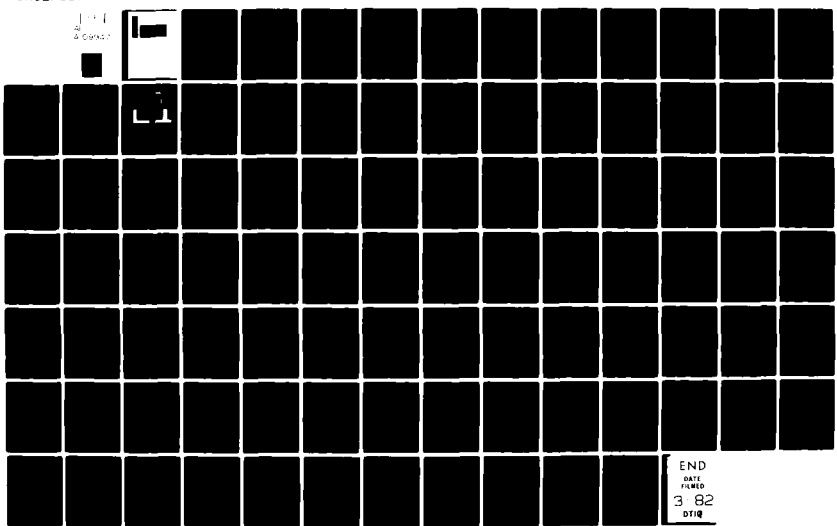
SCIENCE APPLICATIONS INC MCLEAN VA
FLUID DYNAMICS-REACTIVE FLOW MODELING. (U)
DEC 81 E HYMAN, M FRY, J TITTSWORTH, D FYFE
SAI-82-655-WA

F/G 20/4

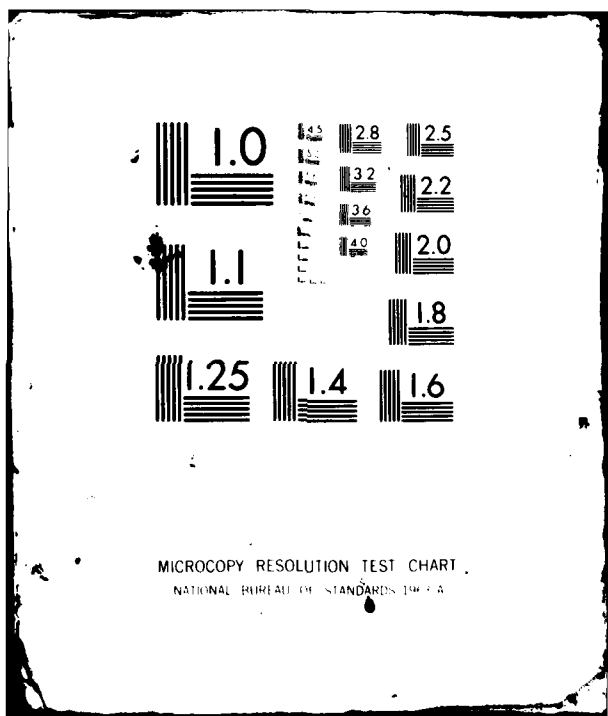
N00014-81-C-2085
NL

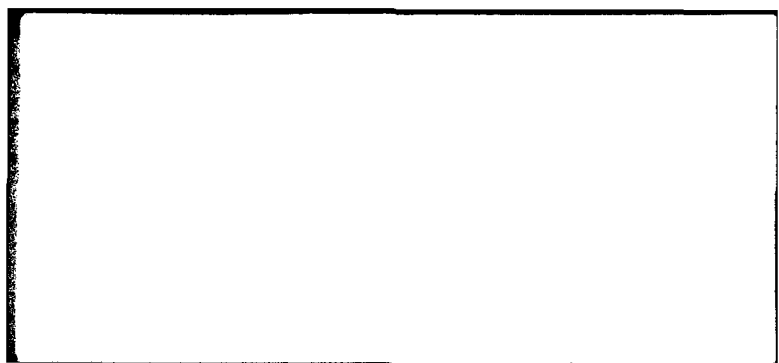
UNCLASSIFIED

100-1
200-2
300-3



END
DATE FILMED
3 82
010





DISCLAIMER NOTICE

**THIS DOCUMENT IS BEST QUALITY
PRACTICABLE. THE COPY FURNISHED
TO DTIC CONTAINED A SIGNIFICANT
NUMBER OF PAGES WHICH DO NOT
REPRODUCE LEGIBLY.**

FLUID DYNAMICS-REACTIVE
FLOW MODELING

Final Report

SAI-82-655-WA

16 Dec 1981

Accession For	
NTIS GRA&I	<input checked="" type="checkbox"/>
DTIC TAB	<input type="checkbox"/>
Unannounced	<input type="checkbox"/>
Justification	
By _____	
Distribution/ _____	
Availability Codes	
Dist	Avail and/or Sp. Ctrl
A	Code 23



FLUID DYNAMICS-REACTIVE
FLOW MODELING

Final Report

SAI-82-655-WA

Submitted to:

Laboratory for Computational Physics
Code 4040
Naval Research Laboratory
Washington, D.C. 20375

Prepared Under:

Contract #N00014-81-C-2085

Prepared by:

Ellis Hyman

with

Mark Fry
Jeff Tittsworth
David Fyfe
K. Kailasanath

SCIENCE APPLICATIONS, INC.

P.O. Box 1303
1710 Goodridge Drive
McLean, Virginia 22102

(703) 734-5840

TABLE OF CONTENTS

	<u>Page</u>
GENERAL DISCUSSION	1
REFERENCES	6
APPENDIX A - SHOCK CAPTURING USING FLUX-CORRECTED TRANSPORT ALGORITHMS WITH ADAPTIVE GRIDDING	A-1
APPENDIX B - A THEORETICAL STUDY OF THE IGNITION OF PRE-MIXED GASES	B-1
APPENDIX C - REVISED SUBROUTINES - INITAL AND RTCON.	C-1

GENERAL DISCUSSION

In the following discussion we will describe the work performed by Science Applications, Inc. (SAI) on contract number N00014-81-C-2085, SAI project number 1-157-18-265, entitled "Fluid Dynamics-Reactive Flow Modeling," which had a technical performance period of 1 December 1980 to 30 November 1981.

This work includes (1) adaptations of the FAST2D code for slow flow applications, (2) use of the FAST2D code to model vorticity and turbulence flow efficiently, (3) an analytical and computational study of the ignition and quenching of laminar flames in a premixed H_2 , O_2 , N_2 mixture, and (4) incorporation of the latest reactive flow computer packages into the NRL ionosphere code. Each of these topics will be described in the following paragraphs.

SAI has recently increased the flexibility and efficiency of FAST2D, a two dimensional hydrocode developed by The Laboratory for Computational Physics at NRL. The transport algorithm used for transporting density, momentum, energy, and chemical species has been altered to compute along as many as ten rows of computational cells at a time. The original algorithm could only accommodate one row at a time. The new algorithm was compared to the original using a cylindrical axisymmetric shear flow problem. Since no changes were made in the differencing scheme itself, the new algorithm gave exactly the same results as the original. A factor of five increase in computing speed was obtained.

In preparation for reactive slow flow modeling FAST2D's mechanism for following chemical species was altered. Number densities rather than fractional densities for all the species are transported in order to make FAST2D compatible with existing chemical reaction schemes and molecular diffusion packages. The revised version has been benchmarked in a non-reacting shear-flow problem similar to the one mentioned above. As a result, no significant numerical diffusion of chemical species occurred.

A project involving shock modeling was also completed using FAST2D. The object of the study was to accurately and efficiently capture the various structures in complex, non-steady shocks. The quasi-Lagrangian rezoning capabilities of FAST2D were sufficient for modeling two of the four cases studied, regular and single mach reflection. Complex and double mach reflections were modeled after an additional rezoning capability was added to FAST2D. The code was modified to allow the grid to expand about any arbitrary point within the computational system. In this way, grid and fluid motions were synchronized such that self-similar shock structures could grow naturally with the system. This work has been reported in Fry, M., et al., "Shock Capturing Using Flux-Corrected Transport Algorithms with Adaptive Gridding," NRL Memo Report 4629 (1981) and appears in this report as Appendix A. This new adaptive gridding technique allows one to more efficiently model vorticity and turbulence flows.

A theoretical and computational study of the ignition and quenching of laminar flames in a premixed $H_2:O_2:N_2$ mixture has been performed and a detailed report of the work, entitled "A Theoretical Study of the Ignition of Pre-Mixed Gases," is included as Appendix B. The objectives

of this work were: (1) to complete the calibration of the similarity solution model, and (2) to utilize the similarity solution model in conjunction with the NRL 1-D flame model to study the ignition, propagation and quenching of laminar flames in premixed gases.

The similarity solution model is based on an analytic similarity solution to the non-linear time-dependent slow flow equations. The similarity solution and the induction time for the fuel-oxidizer mixture as a function of temperature and pressure can be used to calculate whether or not a given energy source is adequate to ignite the system. This simple procedure is then calibrated using the NRL 1-D flame model which includes the thermo-physical properties of the mixture, a full chemical kinetics scheme, nonlinear convection, molecular diffusion and thermal conduction. The details of the calibration are given in Appendix B.

The similarity solution model predicts whether or not a mixture will ignite given the initial radius of energy deposition R_0 , the duration of the heating τ_0 and the total energy deposited in the system E_0 . If ignition is predicted, the model gives the time it takes for ignition to occur. In contrast, the NRL flame model not only predicts ignition, but also provides the structure of the propagating flame. The calculations presented in Appendix B show that the similarity solution predicts ignition accurately when the radius of energy deposition is larger than the quench radius. The NRL flame model is used to estimate the quench radius as well as to explain the discrepancy in the predictions of the two models for very small radii of energy deposition.

SAI has incorporated the latest reactive flow computer packages into the NRL computer code for the

numerical modeling of the mid-latitude ionosphere.⁽¹⁾ There are two significant additions to the code to improve speed and flexibility. Firstly, the ordinary differential equation (ODE) solver, IMPLCT, used to time advance the chemistry part of the continuity equations was replaced by one which takes advantage of the form of the equations. If there are NZ grid points in altitude, then the ODE's decouple into NZ systems since with the time-splitting algorithm used the chemistry at a given altitude will not depend on the chemistry at any other altitude within the one hydrodynamic time step. Doing many systems at once is an ideal situation for a vector computer like the TI-ASC. The computer package, VSAIM, developed at NRL does such a problem. Since the chemistry at one altitude may proceed faster than at another altitude, VSAIM allows each system to use its own time step. After each chemistry time step it terminates those that have reached the desired ending time and if necessary starts a new system thus keeping the vectors as optimally long as possible throughout the computation. VSAIM, like its predecessor, CHEMEQ,⁽²⁾ also tries to treat those equations it deems are difficult to solve with a special algorithm for stiff equations and those which are easy to solve with a simpler algorithm.

The second major incorporation into the 1D ionosphere code is a routine for the processing of chemical reactions and their reaction rates. Formerly these reactions and reaction rates were hard-wired with the program, requiring program modification for even the slightest change in reaction rate coefficients or the number of reactions. By using the automatic rate processor, ARTP, the chemical reactions and their corresponding reaction rates are input as data cards allowing great flexibility in the choice of the type of chemistry one elects to incorporate into the ionospheric model.

In order to make these modifications it was necessary to change the data structures used to store the densities of the various chemical species. Instead of using a distinct array for each specie present in the problem, one larger array indexed by the number of species in the problem is now used. An array of symbols is now used to distinguish one specie from another. These symbols are the data that ARTP uses to recognize which species are involved in each reaction it processes. By making the types of ions and minor neutrals input to the program, the user has a greater flexibility to test the effects of various chemical reactions and the importance of the various ions or minor neutrals on the resulting ionosphere.

While the modifications to the code were being made, documentation describing the variables used by the code was added. Furthermore, a separate piece of documentation was added to describe the input data to the program, making the whole program much more user oriented. In Appendix C we have included the revised versions of 2 subroutines - INITAL and RTCON. These subroutines supply all the information necessary for setting up the input required for making a run of the ionosphere code.

REFERENCES

1. E. S. Oran, T. R. Young, Jr., D. V. Anderson, T. P. Coffey, P. C. Kepple, A. W. Ali, and D. F. Strobel, "A Numerical Model of the Mid-Latitude Ionosphere," NRL Memorandum Report 2839, July 1974.
2. T. R. Young, "CHEMEQ - A Subroutine for Solving Stiff Ordinary Differential Equations," NRL Memorandum Report 4091, February 26, 1980.

Appendix A
SHOCK CAPTURING USING FLUX-CORRECTED TRANSPORT
ALGORITHMS WITH ADAPTIVE GRIDDING

SHOCK CAPTURING USING FLUX-CORRECTED
TRANSPORT ALGORITHMS WITH ADAPTIVE GRIDDING

M. Fry and J. Tittsworth
Science Applications, Inc.
McLean, Virginia, 22102, USA

A. Kuhl
R and D Associates
Marina del Rey, California, 90291, USA

D. Book, J. Boris and M. Picone
Laboratory for Computational Physics
U. S. Naval Research Laboratory
Washington, D.C., 20375, USA

A numerical technique has been developed for capturing complex, nonsteady shock structures in multidimensions. The technique relies on moving the computational mesh with the shock wave so that the features of principal interest appear approximately stationary. The method has been implemented using coordinate-split Flux-Corrected Transport (FCT) algorithms which allow the mesh to evolve arbitrarily with respect to the fluid in each coordinate. The grid may thus be optimized in response to the needs of a given problem. Synchronizing the grid and fluid motions permits significant reduction of numerical transients and eliminates numerical diffusion. Shocks develop naturally, with no fitting. The method is illustrated by calculating complex, two-dimensional Mach reflection phenomena associated with airblasts and shock diffraction on wedges. The numerical results are in good agreement with available experimental data.

INTRODUCTION

Numerical solution of transient multidimensional gas dynamics problems is always nontrivial. When, in addition, the problem involves reflecting supersonic flows, large variations in length scales in both space and time, or phenomena for which neither analytic solutions nor detailed experimental observations are at hand, the state of the computational art is challenged. Such a problem arises in calculating the oblique reflection of shocks from solid surfaces in planar geometries (e.g. shock tube experiments) or axisymmetric geometries (e.g. airblasts). The complications arise mainly from the presence of Mach reflections which occur when a shock front impinges on a reflecting surface at angles of incidence sufficiently far from normal. The formation of a Mach stem and, consequently, of a slip surface intersecting the triple point (the confluence of the incident, Mach, and reflected waves) results from the requirement that the flow behind the reflected shock be parallel to the reflecting surface, which cannot be achieved through regular reflection.

Attempts to calculate the properties of the flow in Mach reflections date back at least to von Neumann¹ and the research which grew out of the wartime explosive studies²⁻⁴. For the simplest problem, that of a planar shock

Manuscript submitted August 24, 1981.

reflecting from a plane surface, Jones, Martin, and Thornhill⁵ noted that it is possible to reduce the number of independent variables to two by transforming to the similarity variables x/t , y/t , a device that was also used by Kutler, et al⁶. Ben-Dor⁷ developed a theory which used shock polars to explain some of the features of this problem, and solved the system of algebraic equations obtained by combining the jump conditions across the various discontinuities (Courant and Friedrichs)⁸ to describe the flow in the neighborhood of the triple point. To date, no satisfactory treatment of the complete flow field has been published, although some features (like the shape of various waveforms) are quite easy to model.

In connection with studies of both chemical and nuclear explosions there have been many attempts to model a spherical blast wave reflecting from the ground, the so-called height-of-burst (HOB) problem. The hydrodynamic phenomena in the two cases are identical, although nonideal effects (primarily explosive afterburn in the first instance and radiation preheating in the second) are different. Previous attempts to model two-dimensional complex shock reflection have suffered from restriction to describing part of the system, the use of a special assumption like that of self-similarity, or less than satisfactory agreement with experimental data.⁹

The calculations discussed here represent a step forward in overcoming these difficulties. They differ from previous numerical work in incorporating two important computational developments: Flux-Corrected Transport (FCT)¹⁰ and an adaptive regridding procedure, called "sliding rezone",¹¹ which optimizes the mesh point distribution and hence the resolution of surfaces of discontinuity.

FCT is a finite-difference technique for solving the fluid equations in problems where sharp discontinuities arise (e.g. shocks, slip surfaces and contact surfaces). It modifies the linear properties of a second- (or higher) order algorithm by adding a diffusion term during convective transport, and then subtracting it out "almost everywhere" in the antidi diffusion phase of each time step. The residual diffusion is just large enough to prevent dispersive ripples from arising at the discontinuity, thus ensuring that all conserved quantities remain positive. FCT captures shocks accurately over a wide range of parameters. No information about the number or nature of the surfaces of discontinuity need be provided prior to initiating the calculation.

The FCT routine used in the present calculations, called JPBFC (an advanced version of ETBFCT)¹², consists of a flexible, general transport module which solves 1-D fluid equations in Cartesian, cylindrical, or spherical geometry. It provides a finite difference approximation to the conservation laws of the general form:

$$\frac{\partial}{\partial t} \int_{\delta V(t)} \phi dV = - \int_{\delta A(t)} \phi \cdot (u - u_g) \cdot dA + \int_{\delta A(t)} \tau dA \quad (1)$$

where ϕ represents the mass, momentum, energy or mass species in cell $\delta V(t)$, u and u_g represent the fluid and grid velocities, respectively, and τ represents the pressure/work terms. This formulation allows the grid to slide with respect to the fluid without introducing any additional numerical diffusion. Thus, knowing where the features of greatest interest are located, one can concentrate fine zones where they will resolve these features most effectively as the system evolves (Fig. 1).

In the next section we describe the computational techniques used to solve the wedge problem and present the results of four simulations carried out to reproduce experimental results of Ben-Dor and Glass.¹³ In Section III we present a parallel discussion for a HOB calculation. Finally, in Section IV we summarize our conclusions.

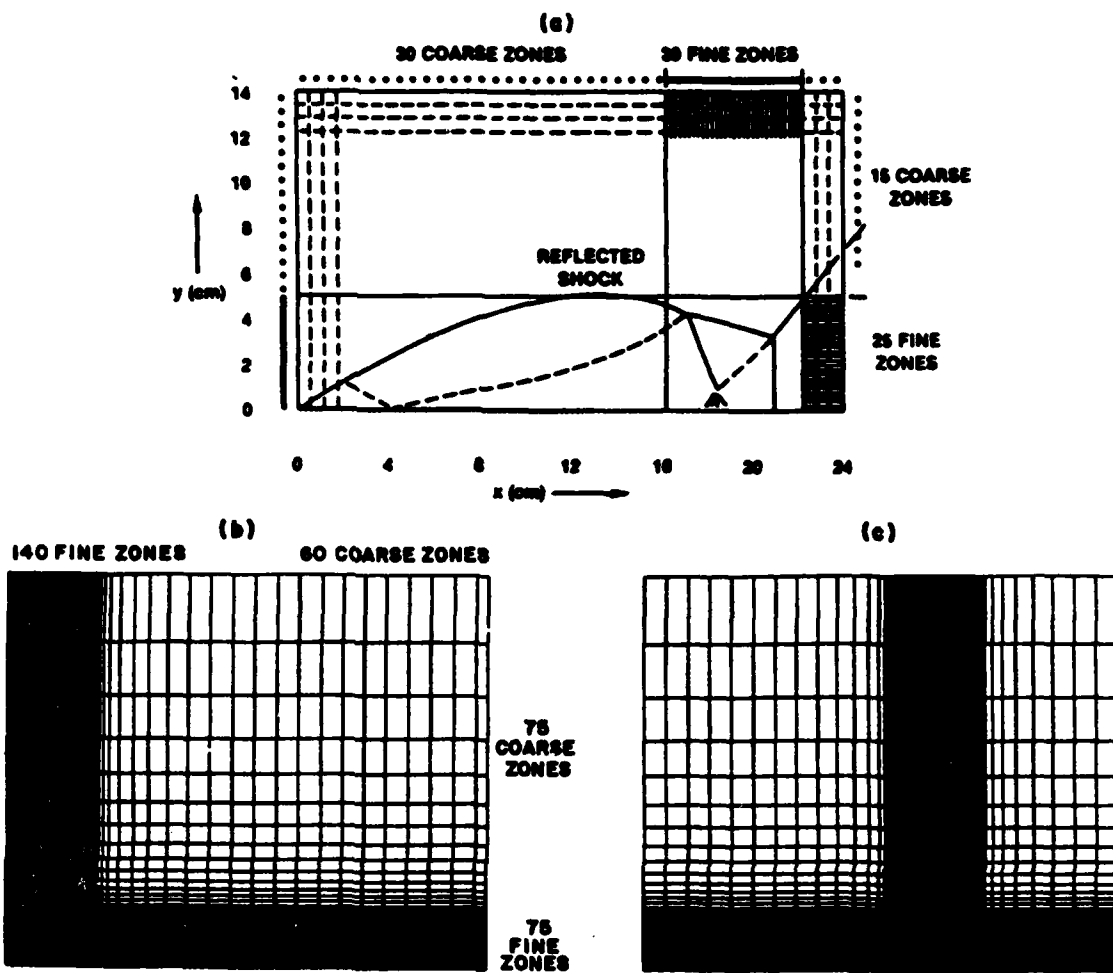


Fig. 1. Adaptive grids for a) planar shocks on wedge (double Mach shock features are indicated); b) and c) HOB problem initially and at transition point (grid lines in fine-zone region are indistinguishable).

SHOCK-ON-WEDGE CALCULATIONS

The JPBFC algorithm was used in a 2-D Cartesian version of the FAST2D code to model the reflections of planar shocks from wedges of 20° to 60° and varying shock strengths. Four general classes which include regular, single, complex and double Mach reflection were calculated (referred to as cases a,b,c,d respectively). The bottom of the mesh, treated as a reflecting boundary, modeled the surface of the wedge. Quantities on the right hand boundary and on the top were set equal to the ambient values. The remaining boundaries were treated as permeable. In the single, complex, and double Mach reflection cases, the mesh was anchored on the left, essentially at the wedge tip where the incident shock first strikes, while the zones were stretched by a scaling factor proportional to t as soon as the reflection region filled a substantial portion of the grid. In case (d), the double Mach reflection case, the opening angle is so small that the incident shock has to traverse many zones before the mach stem has grown large enough to be well resolved. For this reason, the problem was solved on a uniform mesh in the frame of reference fixed

to the reflection point, with stretching being initiated after the first Mach stem reached ~ 20 cells in length. The timestep was recalculated at every cycle with a Courant number of 0.5.

Figure 2 shows the pressure and density contours and the velocity field for cases a,b,c,d. The pertinent shock phenomena can be easily identified: incident shock, contact surface, first and second Mach stems. As shown in Fig. 1, the zoning is particularly sparse except for the region of interest. Adequate resolution of the key surfaces (contact and second Mach stem) is obtained with 5 zones in each direction. The accuracy can be evaluated by comparing the experimental density distributions along the wall (Fig. 3).

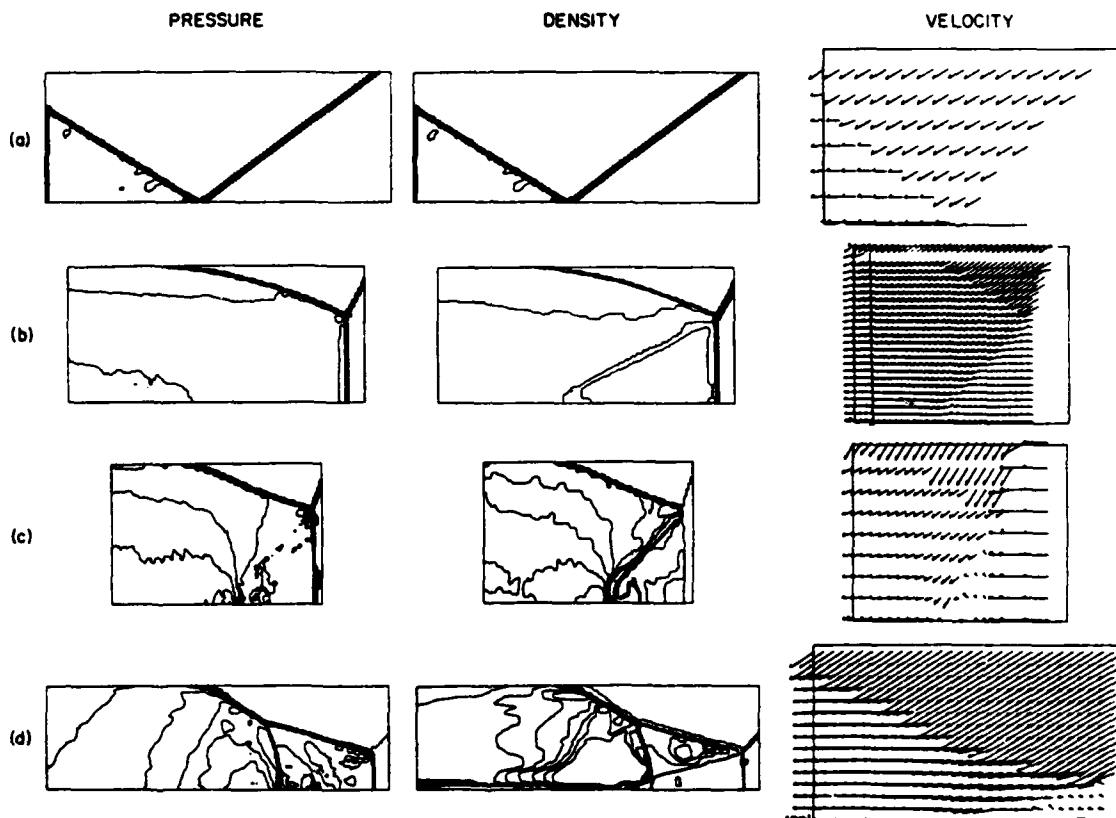


Fig. 2 - Pressure and density contours and flow velocity vectors (in frame of reflection point) for planar waves with Mach number M reflecting from wedges with angle θ for (a) $M=2.03$, $\theta=60^\circ$; (b) $M=2.82$, $\theta=20^\circ$; (c) $M=5.29$, $\theta=30^\circ$; (d) $M=7.03$, $\theta=50^\circ$

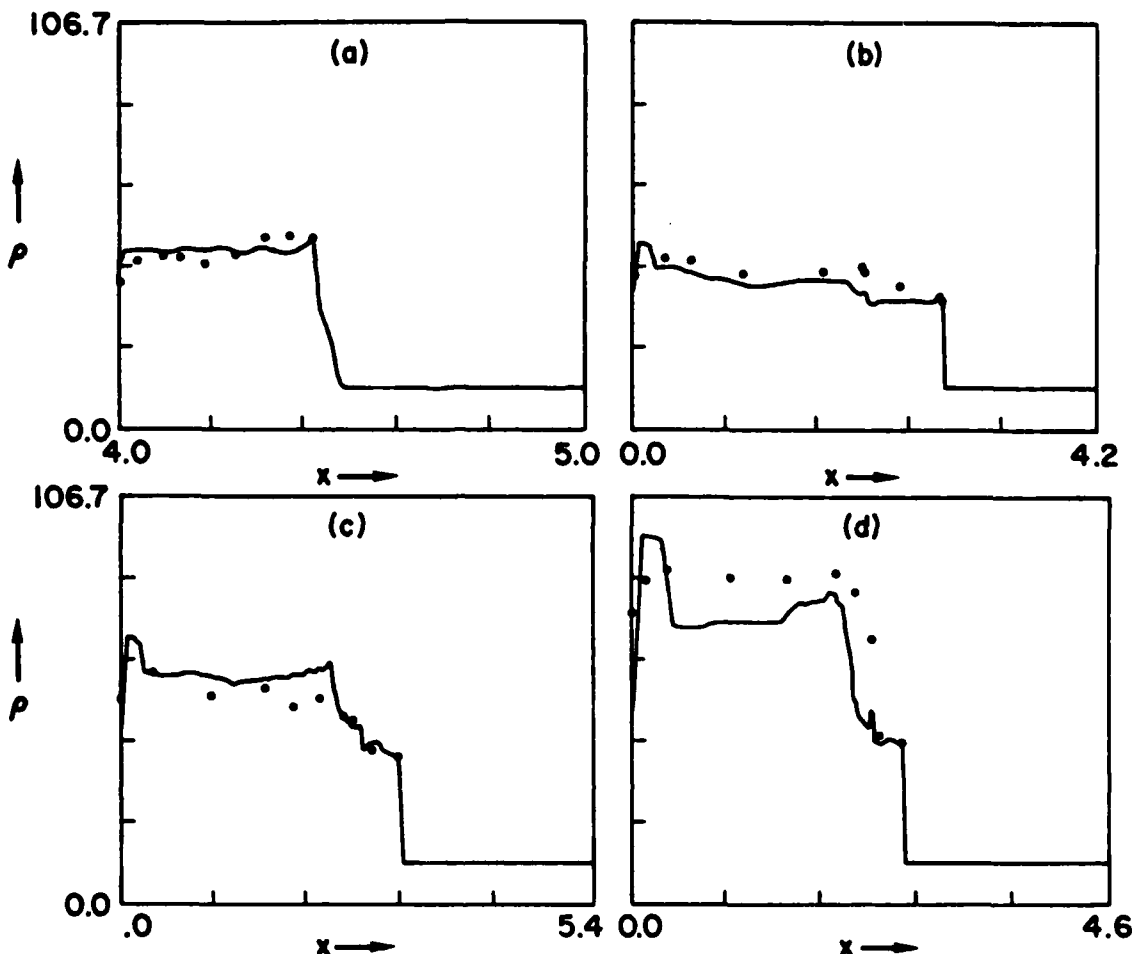


Fig. 3. Comparison of density (in units of ambient density ρ_0) for cases (a), (b), (c), (d) of Fig. 2 vs. distance from corner. Points are measured values reported in Ref. 13.

HEIGHT OF BURST CALCULATIONS

Next, we performed a numerical simulation of a 1KT nuclear detonation at 31.7 m HOB, a case which could be readily compared with high explosive data. A constant ambient atmosphere was used with a density of $1.22 \times 10^{-3} \text{ g/cm}^3$ and pressure $1.01 \times 10^6 \text{ dynes/cm}^2$. To relate the energy and density to the pressure, a real-air equation of state (EOS) was used. This table-lookup EOS was derived from theoretical calculations by Gilmore^{14,15} for equilibrium properties of air and has been vectorized for the Advanced Scientific Computer¹⁶. The internal energy density used in the call to the EOS is found by subtracting kinetic from total energy; this can be negative due to truncation (phase) errors. When this occurred, the value of the pressure was reset to zero.

The transition from regular reflection to double Mach reflection occurs at a ground range approximately equal to the HOB. The size of the mesh should

therefore be roughly twice the HOB in both directions. The upper boundary should be far enough away from the blast front to be non-interfering. We chose boundaries of 55 m for the radial direction and 103.5 m for the axial direction. The fine grid in the radial direction contained 140 out of 200 total zones, each 5 cm in length. The rightmost zones were 80 cm in length, and a smoothing involving 40 zones was performed between the regions to guarantee that the zone sizes varied slowly. In the axial direction the fine grid contained 75 out of 150 total zones, each 5 cm in length. Beyond that region the zones were geometrically increased by a factor of 1.112.

Placement of the fine grid at the origin of the mesh (ground zero, the point at which reflection first occurs) was determined to be optimum for capturing peak pressure in the airblast waveform. Thus, as the expanding wave moves along the ground surface, the fine grid is always locked to it and each point along the blast front encounters the same spatial gridding as it approaches the ground. By treating each point of the incident front in the same manner, we insure that the calculation is internally consistent and that the computed transition point is accurate to within the limits of the resolution.

The initialization provides a strong shock with approximate Mach number M=12. This speed and the need for restart capability led to the choice of 200 timesteps as an interval for the spatial display (snapshots). The dump interval that resulted was $\Delta t \sim 0.3$ milliseconds (ms). These dumps were stored on magnetic tape and post-processed.

A fit to the 1-D nuclear blast flow field (Ref. 17) was used to initialize the energy and mass density and velocity field at 3.76 ms. The corresponding peak overpressure was 113 bars. After the 1 KT flow field was laid down inside a radius of 31.6 m, the fine-zone grid was activated to follow the peak pressure as it moved along the ground surface, modelled as a perfectly reflecting boundary. This region comprised 140 zones, and a switch was set to keep 40 of these zones ahead of the reflection point. Permeable boundary conditions are used on the top and right edges of the mesh, i.e., density, pressure and velocity are set equal to ambient preshock conditions. Reflecting conditions were applied to the left and bottom. The total elapsed physical time in the 2-D calculation, 7.6 ms, required 5600 cycles. Times are referred to $t=0$ at the start of the calculation.

The numerical simulation begins just before the shock first reflects from the ground. Fig. 4a indicates the pressure and density contours and velocity vectors at time 3.18 ms. In Fig. 4b the reflected shock is shown moving upward, the outward flow begins to stagnate at the ground (transition). Fig. 4c, $t=5.99$ ms, shows an enlargement of the shockfront, and the development of the Mach stem, slip surface and second Mach stem. The angle of the shock front with respect to the ground is increasing with time, so that the effective wedge angle is decreasing. From Ben-Dor and Glass¹⁸ one expects a transition to double Mach stem to occur at approximately 45°. The angle in Fig. 4b is about 45° and the shock front has entered the transition phase. Figure 4d shows the fully developed shock structure at 7.79 ms. Clearly visible is the second Mach stem and a vortex region behind the first Mach stem. Toeing out of the first Mach stem can be also seen in the contours of Fig. 4d and occurs as the fluid rolls forward where the slip line would otherwise intersect the ground. The velocity field in Fig. 4d also shows this detail.

One should also note the reflected shock properties. The reflected shock propagates rapidly through the high temperature fireball, due to the high local soundspeed. The shape of this reflected wave is a primary difference between the HOB case and the wedge case¹⁹. The other major difference, of course, is the spherically expanding blast wave which decreases in strength approximately proportional to r^{-2} .

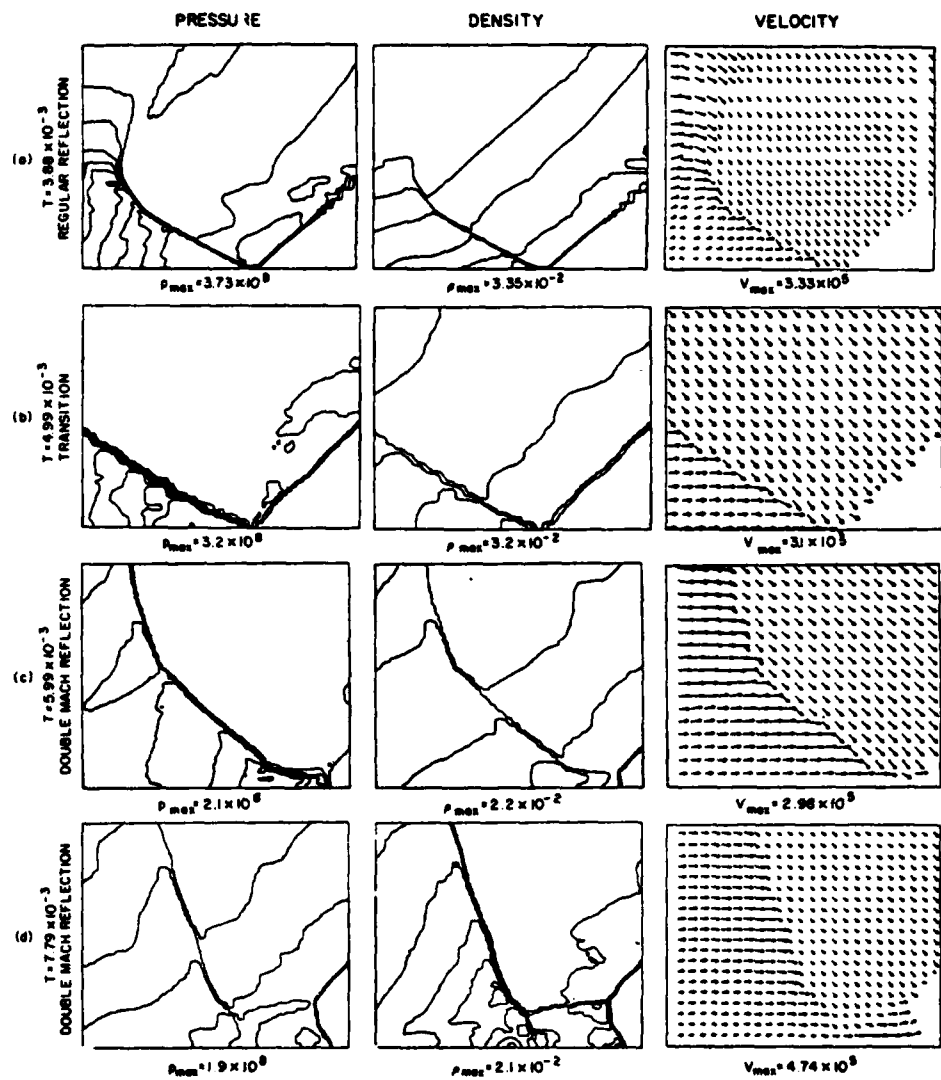


Fig. 4. Pressure, density, and velocity fields for HOB calculation (a) in regular reflection stage; (b) at transition to Mach reflection; (c) shortly afterward, when second peak has become larger than first; and (d) fully developed (note toe at base of first Mach stem).

Finally we consider the pressure/distance relation for the HOB case. In Fig. 5 we compare the results of the numerical simulation with the data of Carpenter and with empirical analysis. Carpenter's data are based upon careful HOB experiments with 8 lb PBX9404 spheres. The empirical analysis was based on a 1 KT nuclear free air curve and HOB construction factors. The calculated values in the regular reflection regime are 20% low and may be attributed to a combination of FCT clipping, the resolution of the grid, and inaccuracies in the initialization of the flow field. During and after Mach reflection, the peaks remain low until the Mach stem structure has grown large enough to be resolved on the mesh. By the time it occupies a region of 15 cells high and 35 cells wide, the peak pressures are in good agreement with the HE data and the empirical analysis.

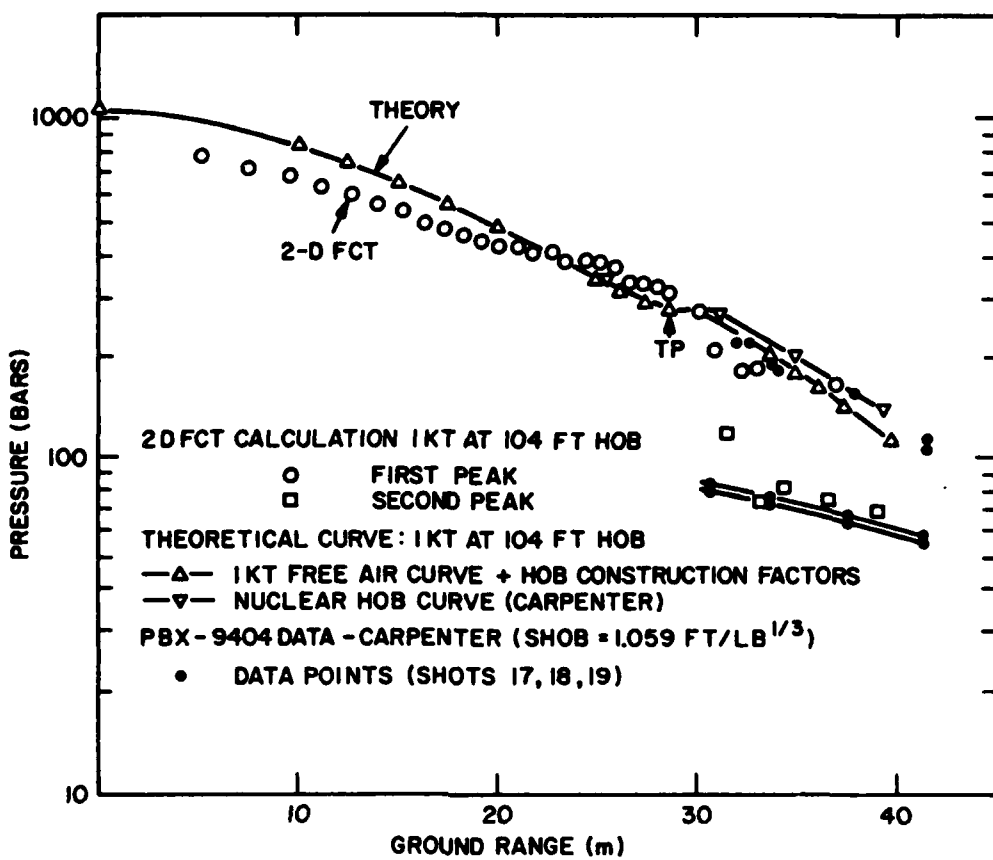


Fig. 5. Pressure-range curves for first and second (after transition - denoted by TP - to double Mach reflection) peaks.

SUMMARY AND CONCLUSION

The complex 2-D Mach reflection phenomena associated with shock diffraction on wedges and height-of-burst explosions have been modeled with the FAST2D computer code. Four wedge cases—regular, single, complex and double Mach reflection—have been calculated and the results compared to experiments. A nuclear detonation (1 KT at 31.7m HOB) was also simulated. The results give insight into the formation and subsequent evolution of the Mach stem, the triple point and the contact discontinuity. The transition from regular reflection to double Mach reflection is predicted. Excellent agreement with Ben-Dor's data is obtained. We suggest that the first signal for transition is the appearance of a second peak behind the shock front due to stagnation in the flow. Calculated first and second pressure peaks versus distance in the HOB case agree both with the HE data and analysis to within 20%.

The use of the adaptive regridding procedure, called "sliding rezone", along with the FCT algorithm allows one to accurately predict the nonsteady shock structures in two dimensions for diffractions on wedges and HOB cases. Comparison with data for both wedges and HOB yields the best results obtained to date.

ACKNOWLEDGEMENT

This work was supported by the Defense Nuclear Agency under Subtask Y99QAXSG, Work Unit 00001, and Work Unit Title "Flux-Corrected Transport."

REFERENCES

1. Von Neumann, J., "Oblique Reflection of Shocks", Explosive Research Report No. 12, Navy Department, Bureau of Ordnance, Re2c, Washington, D.C. (1943).
2. Taub, A. H., "Refraction of Plane Shock Waves", Rev. Mod. Phys., Vol. 21, p. 51 (1947).
3. Bleakney, W., and Taub, A. H., "Interaction of Shock Waves", Rev. Mod. Phys., Vol. 21, p. 584 (1949).
4. Lighthill, M. J., "On the Diffraction of Blast I", Proc. Roy. Soc., Vol. 198, p. 454 (1949), Vol. 206, p. 554 (1950).
5. Jones, D. M., Martin, P. M., and Thornhill, C. K., "A Note on the Pseudo-Stationary Flow Behind a Strong Shock Diffracted or Reflected at a Corner", Proc. Roy. Soc., Sec. A, Vol. 225, p. 238 (1951).
6. Shankar, V., Kutler, P., and Anderson, D., "Diffraction of a Shock Wave by a Compression Corner - Part II, Single Mach Reflection", AIAA Journal, Vol. 16, No. 1 (1977).
7. Ben-Dor, G., and Glass, I., "Nonstationary Oblique Shock Wave Diffractions in Nitrogen and Argon - Experimental Results", UTIAS Tech Note (1978).
8. Courant, R., and Friedrichs, K. O., "Supersonic Flow and Shock Waves", Interscience Publishers, New York (1948).
9. Booën, M., and Needham, C., "Two-Dimensional Hull Code Simulation of Complex and Double Mach Reflections", AFWL NTE TN 81-001 (1981).
10. Boris, J., and Book, D., "Flux-Corrected Transport: I SHASTA, A Fluid Transport Algorithm that Works", J. Comp. Phys., 11, 38 (1973).
11. Oran, E. S., Young, T. R., Jr., and Boris, J. P., "Applications of Time-Dependent Numerical Methods to the Description of Reactive Shock", Proc. 17th Symposium (International) on Combustion, The Combustion Institute, Pittsburgh (1979).
12. Boris, J. P., "Numerical Solution of Continuity Equations", NRL Memo Report 3327 (1976).
13. Ben-Dor G, and Glass, I., "Domains and Boundaries of Non-Stationary Oblique Shock-Wave Reflections, II Monatomic Gas", J. Fluid Mech., 96, p. 735 (1980).
14. Gilmore, F. R., "Equilibrium Composition and Thermodynamic Properties of Air to 24,000°K" RAND Corp, RM-1543 (24 August 1955).
15. Gilmore, F. R., "Equilibrium Thermodynamic Properties of High Temperature Air", Lockheed Missile and Space Co., DASA 1917-1 (April 1967).
16. Young, T. R., (Private Communication 1981).
17. Needham, C., et. al., Nuclear Blast Standard, AFWL 7R-73-55, Air Force Weapons Laboratory (April 1975).
18. Ben-Dor, G., Glass, I., "Domains and Boundaries of Non-Stationary Oblique Shock-Wave Reflections Diatomic Gas", J. Fluid Mech., Vol. 92, part 3, p. 459 (1979).
19. Book, D., et. al., "Two-Dimensional FCT Model of Low Altitude Nuclear Effects", NRL Memo Report 4362 (1980).
20. Carpenter, H. J., "Height of Burst at High Overpressures", 4th International Symposium on Military Applications of Blast Simulation (1974).

Appendix B
A THEORETICAL STUDY OF THE
IGNITION OF PRE-MIXED GASES

by:

K. Kailasanath
Science Applications, Inc.
McLean, Virginia 22102

and

E. Oran and J. Boris
Laboratory for Computational Physics
Naval Research Laboratory
Washington, D.C. 20375

ABSTRACT

In this paper, time-dependent results obtained from both a simple but nonlinear analytic similarity solution and a detailed numerical simulation model are used to study the interactions between the fundamental processes occurring in the ignition of homogeneous premixed gases. The parameters which may be varied are the composition of the mixture, the initial radius of energy deposition R_0 , the duration of the heating T_0 , and the total energy deposited in the system E_0 . The similarity solution plus the induction time for the fuel-oxidizer mixture as a function of temperature and pressure can be used to calculate whether or not a given energy source is adequate to ignite the system. This simple procedure is then calibrated using a time-dependent detailed numerical reactive flow model which includes the thermophysical properties of the mixture, a full chemical kinetics scheme, nonlinear convection, molecular diffusion and thermal conduction. Calculations are presented for a selected mixture of $H_2-O_2-N_2$ for various values of R_0 and E_0 . These show that the similarity solution predicts ignition accurately when the radius of energy deposition is larger than the quench-radius. The detailed numerical reactive flow model is used to predict the quench-radius and the absolute minimum ignition energy associated with it.

NOMENCLATURE

A	Nonlinear amplitude in similarity solution
E	Energy
E_0	Total amount of energy deposited
I	Induction Parameter
k	Scale size in similarity solution
k_B	Boltzmann's constant
N	Total number density
n_j	Number density of species j
P	Pressure
P_j	Term representing production of species j
Q_D	Contribution to the heat flux vector due to diffusion
Q_j	Term representing loss of species j
R_0	Initial radius of deposition
R_c	Characteristic radius of energy deposition
r	Radial distance
T	Temperature
t	time
v	fluid velocity
v_j	Diffusion velocity of species j
γ	ratio of specific heats, c_p/c_v
η_m	mixture viscosity coefficient
λ_m	mixture thermal conductivity coefficient
ρ	mass density
τ_0	time period during which energy is deposited
τ_c	chemical induction time

INTRODUCTION

An external source of energy can initiate interactions among the controlling convective, diffusive and chemical processes in a fuel-oxidizer mixture. Whether the interactions result in ignition of a deflagration or detonation wave depends on the intensity, duration, and volume affected by the external heat source. Ignition will also depend on the initial ambient properties of the mixture which determine the chemical induction time and the heat release per gram of material. Thus ignition is a complicated phenomena whose occurrence for a specific mixture of fuel and oxidizer depends strongly on diffusive and chemical parameters which are often very poorly known.

It is possible, in principle, to study flame ignition by performing detailed numerical simulations. This is a complicated, multi-dimensional, multi-species, time-dependent problem which has been solved in certain limited cases (see e.g., Ref. 1). Part of the complication and cost of such calculations arises from the multi-dimensional solution of the conservation equations, but at least as much arises from integrating the large number of ordinary differential equations describing the chemical reactions. This latter factor is further complicated by the fact that we usually do not have an adequate representation of the chemical reactions with which to work. Thus a convenient, inexpensive way to estimate whether a mixture will ignite given a heat source intensity, duration, and volume would be a very valuable laboratory tool and a useful learning device.

This paper represents an extension and clarification of the work described by Oran and Boris [1,2]. They presented a preliminary summary of a simplified, theoretical model of localized ignition of a homogeneous, premixed gas and explained how it could be calibrated by using a detailed simulation. In this paper the calibration of the simplified model is extended and the results are compared in detail to those of detailed, one-dimensional simulations. After a brief review of related literature, the essential properties of the detailed, time-dependent, numerical model are presented. Then a description is given of a closed form similarity solution for the nonlinear time-dependent slow flow equation which forms the basis for the simplified model of localized ignition. The similarity model avoids the integration of the ordinary differential equations describing the chemical reactions by defining an induction parameter. Two constants must be calibrated; the radius at which the thermal conductivity is evaluated and the radius at which the induction parameter is evaluated. Finally, comparisons between the two models are described for ignition of a $H_2-O_2-N_2$ mixture. The composition of the mixture and the duration of energy deposition are held constant but the total energy deposited and the radius of deposition are allowed to vary.

BACKGROUND

Ignition phenomena and the associated properties of minimum ignition energies and quench volumes have been studied both experimentally and theoretically. Lewis and von Elbe [3] have reported extensive experimental data on ignition by electric sparks. Weinberg and Wilson [4] and Kingdon and Weinberg [5] have compared the ignition energies required when a spark and a laser were the source of ignition. The former paper [4] concludes that the laser minimum ignition energy is very much less than that required by a spark for mixtures at low pressures or near the flammability limit. They have attributed this difference to the influence of the electrodes and the losses to them since the quenching distances are large under the above conditions. The latter paper [5] concludes that for short pulses applied to mixtures with small quenching distances, the energies required by the two ignition sources are not that different.

Dixon-Lewis and Shepherd [6] have used a time-dependent flame model to examine the effects of varying the initial radical concentration and of changing the geometry of the initial hot core. Their studies were done on a homogeneous premixed 60% hydrogen-air mixture in which energy was deposited instantaneously in the form of hydrogen atom radicals and temperature. They found that energy in the form of hydrogen atoms was more efficient at igniting a flame. Dixon-Lewis [7] then looked for a minimum quench volume in the same 60% hydrogen-air mixture in which one third of the added energy was in the form of hydrogen atoms.

Another point noted by both Overley et al. [8] and by Dixon-Lewis and Shepherd [6] is that the shape and size of the mixture core is important in determining the minimum ignition energy. The former paper presented a study of a hydrazine mixture in both spherical and prolate spheroidal coordinates. The latter paper considered both cylindrical and spherical systems. Both papers investigated the effects of flame curvature on burning velocity.

The work of Ballal and Lefebvre [9] is a detailed experimental investigation of the effects of pressure, velocity, turbulent intensity and scale, and mixture composition on the minimum ignition energy and quench distance in a flowing gas mixture. Using the data as a guide, they analyzed the important transport and turbulent processes and developed a highly simplified model for the quench distance in the limit of low and high turbulence. The data has allowed them to calibrate the model and determine important constants.

THE DETAILED NUMERICAL SIMULATION MODEL

This section describes the detailed numerical flame model which solves the time-dependent conservation equations for total mass ρ , momentum $\rho\mathbf{v}$, energy E , and individual species densities n_j [2,10]:

$$\frac{\partial \rho}{\partial t} = -\nabla \cdot \rho\mathbf{v} \quad (1)$$

$$\frac{\partial n_j}{\partial t} = -\nabla \cdot n_j\mathbf{v}_j - \nabla \cdot n_j\mathbf{v} + p_j - Q_j n_j \quad (2)$$

$$\frac{\partial \rho\mathbf{v}}{\partial t} = -\nabla \cdot (\rho\mathbf{v}\mathbf{v}) - \nabla p + \nabla \cdot n_m [\nabla\mathbf{v} + (\nabla\mathbf{v})^T] \quad (3)$$

$$\frac{\partial E}{\partial t} = -\nabla \cdot E\mathbf{v} - \nabla \cdot (p\mathbf{v} - \lambda \frac{\nabla T}{m} - Q_D) \quad (4)$$

The technique for solving the various terms in these equations is based on the method of asymptotic timestep splitting in which the individual chemical and physical processes are integrated separately and then asymptotically coupled together [1]. The model permits a wide variety of geometric, initial, boundary and time-varying energy input conditions and was specifically developed to study the various physical and chemical processes which control flame initiation and quenching. [23].

The convective transport is solved by the algorithm ADINC, a Lagrangian hydrodynamic algorithm which solves implicitly for the pressures [11]. The method allows for arbitrary equations of state, gives an accurate representation of material interfaces, and allows steep gradients in species and temperature to be developed and maintained.

A number of tests of this algorithm have been documented by Boris [11]. An adaptive gridding method has been implemented in which cells are inserted or deleted according to externally specified physical conditions in the flow. The diffusion velocities are calculated using an iterative algorithm [12,1].

The chemical interactions are described by a set of nonlinear coupled ordinary differential equations. For this ignition study we have used the H_2-O_2 reaction scheme [13] given in Table 1 which involves the eight reactive species, H_2 , O_2 , O , H , OH , HO_2 , H_2O_2 , H_2O and diluent which is chosen to be N_2 . The thermochemical properties of these species were taken from the JANAF tables [14]. The ordinary differential equations describing the chemical kinetics are solved using a fully vectorized version of the selected asymptotic integration method, CHEMEO, developed by Young [15,16].

Results from a typical flame calculation in spherical geometry are presented in Fig. 1. The figure depicts the time history of the temperature profile after $4mJ$ of energy is deposited over a period of 10^{-4} seconds. Even after the energy deposition is stopped the "core" temperature continues to increase due to the heat released in chemical reactions. With time, however, the temperature near the center decreases and the temperature away from the center increases due to heat conduction. In this case, since the rate of heat generation is greater than the rate of heat loss, the temperature profile develops into that of a typical flame temperature profile. Species profiles and details of the flame front have been presented elsewhere [2].

THE SIMILARITY SOLUTION

The similarity solution is derived from the slow flow approximation [1,17] and is predicated on the assumption that energy addition to the system is slow enough so that there is no shock heating. Thus the system is characterized by flow velocities which are small compared to the speed of sound, and an essentially constant pressure field. The energy and velocity equations may be written in terms of total derivatives as

$$\frac{dp}{dt} \approx 0 = - \gamma p \underline{\nabla} \cdot \underline{v} + \underline{\nabla} \cdot \gamma N k_B \kappa \nabla T + S(t) e^{-\kappa^2(t) r^2} \quad (5)$$

and the continuity equation is written in the form

$$\frac{1}{\rho} \frac{dp}{dt} = - \underline{\nabla} \cdot \underline{v}. \quad (6)$$

In Eq. (5) γ is held constant, and κ is a function of the mixture thermal conductivity, λ_m ,

$$\kappa \equiv \frac{\gamma-1}{\gamma N k_B} \lambda_m(T). \quad (7)$$

The last term on the right hand side of Eq. (5) is the source term. Proper choice of $S(t)$ ensures that a given amount of energy, E_0 , is deposited in a certain time, τ_0 . It is the choice of this Gaussian profile which allows us to obtain the "closed" form similarity solution which is given below.

The details of the solution of Eqs. (5) and (6) are given in the Appendix at the end of this paper. The final results for the temperature and density as a function of time and position may be written as

$$T(r,t) = T_\infty e^{A(t)e^{-k^2(t)r^2}} \quad (8)$$

and

$$\rho(r,t) = \rho_\infty e^{-A(t)e^{-k^2(t)r^2}} \quad (9)$$

where T_∞ and ρ_∞ are the background temperature and density, respectively.

In addition, two ordinary differential equations describing the evolution of $A(t)$ and $k(t)$ are required to complete the solution,

$$\frac{dk}{dt} = -kv_1 - 2ck^3 \quad (10)$$

$$\frac{dA}{dt} = \frac{S(t)}{\gamma P_\infty} - 2ck^2 A \quad (11)$$

where v_1 is an approximation to the velocity based on the assumption that $v(r,t) \equiv v_1(t)r$; and c is a constant which depends upon the configuration of the problem ($c = 1$ for cartesian, 2 for cylindrical and 3 for spherical coordinates). By comparing the results from this similarity solution model to those from the detailed numerical simulation model described earlier, we have seen that the linear dependence on r is a valid approximation before ignition occurs.

The model requires one further definition in order to predict ignition. The chemical induction time, which is a function of temperature and pressure, must be used to define the induction parameter,

$$I(T,P) = \int_0^t \frac{dt'}{i_c[T(r,t'), P(r,t')]} \quad (12)$$

For the work presented in this paper, pressure is constant throughout the calculation. Then $I(T, P_\infty)$ is integrated in time according to Eq. (12). Ignition "occurs" when $I(T, P_\infty) = 1$, which is an exact result in the limit of large heat source and constant temperature near the center of the heated region. Values of τ_c have been calculated [13] for a wide range of temperatures and pressures from the chemical rate scheme given in Table I. In general, τ_c as required in these calculations may be obtained from such detailed kinetic calculations, a few measured points, or from educated guesses. The concept of an induction parameter has been extended in scope and used extensively for reactive shock and detonation studies [e.g., 1, 18, 22].

The parameter κ in Eqs. (10) and (11) is found using the definition in Eq. (7). Determining the temperature (radius) at which κ is to be evaluated is part of the calibration to be done. For this, the derivation in the appendix was also done for the case where κ was assumed to be a function of radius (r). This analysis indicated that if κ is to maintain its similarity form and be a function of time alone, κ must be independent of r . Thus, within the framework of the similarity solution, the appropriate location at which to evaluate κ is at the center ($r = 0$). Determining the location at which the induction parameter, $I(T, P_\infty)$, should be evaluated is the second calibration to be done. This has been done by comparing the predictions of the two models and is discussed in the next section.

In summary, the approximations to Eqs. (1) - (4) which allows us to write Eq. (5) and obtain the solutions represented by Eqs. (8) - (11) are:

1. The flow velocities characteristic of the system are small compared to the speed of sound;
2. The pressure is essentially constant everywhere;
3. The ratio of specific heats, γ , is constant;
4. Molecular diffusion effects are not important until after ignition;
5. The velocity, $V(r,t)$ may be approximated by $V_1(t)r$;
6. The system is homogeneous and premixed;
7. The energy is input in a Gaussian form with a characteristic radius R_c which increases in time; and
8. The gas never gets hot enough to radiate away a significant fraction of its energy during the ignition period.

MODEL COMPARISONS

The calibration of the similarity model is complete when the location at which the induction parameter should be evaluated is determined. For this purpose, the results from detailed simulations are compared to those from the similarity model. Energy deposition in both models is linear in time at a rate determined by requiring an energy E_0 to be deposited in a time τ_0 . For all of the results discussed in this paper, τ_0 is taken to be 10^{-4} seconds. As in the similarity model, energy deposition in the detailed model is in the form of a Gaussian profile in space. The characteristic radius of the Gaussian, R_c , increases with time and is determined in the detailed simulation by the formula:

$$R_c^2 = \frac{2 \int r^2 \ln(T/T_\infty) dr}{\int \ln(T/T_\infty) dr} \quad (13)$$

The chemical model for these first tests was taken to be a mixture of H_2 : O_2 : N_2 in the ratio 2:1:10 at 1 atm and $T_\infty = 300^\circ K$. The induction time as a function of temperature for this mixture was derived from the detailed studies of the H_2 - O_2 reaction mechanisms [13] and is shown in Fig. 2.

In the similarity model, κ was estimated by comparing the formula at $300^\circ K$,

$$\lambda_M^S = \frac{8.4 \times 10^3}{\sigma^2} \sqrt{\frac{T(^\circ K)}{\bar{M}}} \frac{\text{erg}}{\text{cm sec}^\circ K}, \quad (14)$$

which assumes that an average molecular distance $\bar{\sigma}$ and an average molecular weight \bar{M} may be found, to the more exact formulation

$$\lambda_m = \sum_j \lambda_j \left[1 + \frac{1}{2\sqrt{2}} \sum_{k \neq j} n_k w_{jk} \right]^{-1} \quad (15)$$

where w_{jk} is a function of $\{\lambda_j\}$ and the atomic masses $\{m_j\}$ suggested by Mason and Saxena [19]. This gives us

$$\bar{\sigma} = 3.16 \text{ \AA}$$

(16)

$$\bar{M} = 24.3.$$

This approximation is valid because the similarity solution is only accurate for ignition, that is, before any major amount of product or intermediates are formed. Then the parameter κ is found using the definition in Eq. (7). As discussed in the previous section, for the similarity solution κ is evaluated at the central ($r=0$) temperature. In contrast the detailed simulation uses Eq. (15) to evaluate the thermal conductivity at each cell at each time step.

In the first case studied, the initial radius of deposition, R_0 , was 0.1 cm and both models were configured for spherical symmetry. By varying E_0 and evaluating the induction parameter $I(T, P_\infty)$ at the central temperature ($r=0$) the similarity solution indicates that the minimum ignition energy is about 3.7mJ. Figure 3 shows the typical behavior of the amplitude, $A(t)$, and the characteristic radius, R_c , for this test case. If $I(T, P_\infty)$ is evaluated at $R = 0.06$ cm the minimum ignition energy predicted is about 5.1mJ, and if it is evaluated at R_c ignition is not predicted even when E_0 is raised to 8mJ. By comparing these predictions with those from the detailed simulation model we determine the location at which $I(T, P_\infty)$ must be evaluated. Results from the detailed simulation are shown in Fig. 4 for three values of E_0 . Ignition occurs when E_0 is greater than or equal to 3.7mJ. Therefore good agreement between the two models for the case under study is achieved by evaluating the induction parameter at the central temperature.

The central temperature and the induction parameter have been shown for three values of E_0 in Figs. 5 and 6 respectively. The time at which ignition occurs ($I = 1.0$) is shown by a '*' in Fig. 6. A comparison with the

results from the detailed simulation (Fig. 4) tells us that both models predict ignition at essentially the same time for a range of input energies. The temperature profiles predicted by the two models are presented in Fig. 7. The agreement is very good except for long times when the detailed simulation predicts higher temperatures than those from the similarity model. This is primarily due to the heat released in chemical reactions which is not included in the similarity model. It is interesting to note that the effects of molecular diffusion included in the detailed simulation model are not considered in the similarity solution model. The results presented have shown that these effects are not as important as the effects of thermal conduction in determining the ignition characteristics of the system under investigation.

The models were then re-configured for cylindrical geometry and the case, $R_0 = 0.1\text{cm}$, was again investigated. By varying E_0 , the similarity solution indicates that the minimum ignition energy is about 3.5mJ/cm , not very different from the spherical case. The detailed simulation predicts that the minimum ignition energy is between 3.3 and 3.7mJ/cm , so again the predictions of both models are comparable when the induction parameter is evaluated at $r=0$.

EFFECT OF QUENCHING DISTANCE

As discussed in the previous section, good agreement between the predictions of the detailed simulation and the similarity solution is obtained for the case, $R_o = 0.1$ cm. In order to determine if the agreement is good for other values of R_o , various cases were studied and these have been summarized in Table II. Evaluating the induction parameter at the central temperature provides agreement between the ignition predictions of the two models for all the cases in which R_o is greater than 0.1 cm. However, for radii smaller than 0.1 cm the similarity solution predicts a minimum ignition energy that is lower than for the $R_o = 0.1$ case described above. In fact, as the initial radius of deposition decreases below 0.1 cm the similarity solution (with $I(T, P_\infty)$ evaluated at a fixed radius) predicts that the minimum ignition energy also decreases. The detailed simulation does not agree with this prediction. The radius 0.1 cm appears to be a "critical radius" below which the minimum ignition energy again increases. The above observation is similar to that made by Blanc, Guest, von Elbe and Lewis [20]. In their study of spark ignition, it was observed that there was a "critical electrode spacing" below which the minimum ignition energy increased. The critical electrode spacing was termed the "quenching distance".

To study the phenomena of "absolute" minimum ignition energies and quenching distances, the energy deposition in the detailed simulation needs to be modified. Up to this point energy was deposited in a Gaussian profile with a characteristic radius which increased with time. This was necessary in order to ensure that energy was deposited in a manner which closely matches the one derived from the similarity model. In the similarity model,

a Gaussian profile with characteristic radius increasing in time was essential to obtain the similarity solution described earlier. However, for studying the effect of the radius of deposition on the minimum ignition energy, it is confusing to have a varying radius of deposition. Therefore, for the results discussed below, energy is deposited in a Gaussian profile with a constant radius of deposition. As before, energy deposition is linear in time at a rate determined by requiring an energy E_0 to be deposited in a time τ_0 .

For a particular radius of deposition, a certain amount of energy is deposited and the computations are carried out for sufficient time until the existence (or absence) of a propagating flame is definite. By repeating the computations for different values of E_0 a bound for the minimum ignition energy for that particular radius is obtained. Similar calculations are performed for different values of the radius of deposition, R_0 . The results of such investigations are shown in Fig. 8. A propagating flame results when 3.8 mJ of energy is deposited in a sphere with a radius of 0.1 cm. However if the same amount of energy is deposited in a sphere of smaller radius, the rate of heat liberation is insufficient to compensate for the rate of heat loss and consequently there is no ignition. This radius, 0.1 cm, is the "quench-radius" for this particular mixture. For radii slightly larger than the quench-radius, the minimum ignition energy is almost constant and for larger radii (larger than 0.11 cm) the minimum ignition energy increases rapidly with increasing radii. Therefore for the system under study, the

absolute minimum ignition energy is about 3.7 mJ. These observations are in qualitative agreement with those of Lewis and von Elbe [21]. Quantitative comparisons are not possible since the composition of the mixture and the time for energy deposition are different.

This study of the "quench-radius" provides the insight needed to explain the discrepancy in the predictions of the similarity solution and the detailed model for small radii. We conclude that a volume smaller than the "quench-volume" needs to be maintained at a temperature T for a time which is longer than the corresponding induction time for ignition to occur. Therefore the concept of an induction parameter as it is used in the similarity solution is not valid for very small radii. If the absolute minimum ignition energy is deposited in a sphere of radius smaller than the quench radius, ignition will not occur since the heat generation rate within this smaller volume cannot compensate for the heat loss rate. This effect is not significant in measurements of induction time which are for larger radii. Therefore an agreement between the predictions of the two models can be forced for radii smaller than the quench-radius by evaluating the induction parameter at increasingly larger radii (i.e. lower temperatures). For example, when the initial radius of deposition is 0.08 cm, the detailed simulation predicts that the minimum ignition energy is between 3.4 and 5 mJ. The minimum ignition energy predicted by the similarity solution is 3.4 mJ if the induction parameter is evaluated at 0.06 cm and it is 5.1 mJ if the induction parameter is evaluated at 0.08 cm. For the case when the quench radius, $r_q = 0.1$ cm, the formula

$$r = r_q - Ae^{-\frac{BR}{q}}, \quad (17)$$

$A = 2.84 \times 10^{-4}$ and $B = 58.78$ gives a good estimate for the radius at which to evaluate the induction parameter. We are currently seeking a more general formula to give this radius.

SUMMARY AND CONCLUSIONS

This paper describes a theoretical model for flame ignition based on a similarity solution which may be used to predict the ignition properties of a homogeneous mixture of gases. The model requires specification of the amount of energy input, E_0 , the length of time over which the energy is deposited, τ_0 , and the radius of energy deposition, R_0 . The model also requires basic information about the gas mixture which includes estimates of the thermal conductivity and the chemical induction time of the gas mixture as functions of temperature. Since a number of approximations have been applied to derive the model, it has been calibrated and its range of validity determined. This has been done by comparing its predictions to those of detailed numerical simulations.

The one-dimensional detailed numerical simulation used solves the set of coupled partial differential equations representing conservation of mass, momentum, and energy as well as individual species densities. For this study it was configured with an open boundary at one end to simulate an infinitely large system. Energy was deposited linearly with time, as it was done in the similarity solution, and the radius of deposition was chosen to mimic that determined by the characteristic radius in the similarity solution. The detailed model, however, contained calculations of the thermal conductivity and chemical kinetics which were much more accurate than the approximations used in the similarity solution. Furthermore, the detailed model contained the effects of molecular diffusion, which were not at all included in the similarity solution.

Predictions from the similarity model consist of an answer as to whether or not a given mixture would ignite given E_0 , τ_0 , and R_0 . Then if ignition is predicted, the model gives the time it takes for ignition to occur. In

contrast, the detailed simulation model not only predicts ignition, but also provides the structure of a propagating flame.

Comparisons of the predictions of the two models show that the system center is the optimal location for evaluation of an induction parameter, which is the indicator of ignition in the similarity model. Furthermore, the predictions of the similarity model are excellent when energy is deposited in a large enough volume. When the radius of deposition is less than the quench radius of the system, the similarity model is not accurate: the similarity model predicts ignition when the detailed model shows it does not occur. This can be compensated for by evaluating the induction parameter away from the system center. However, as with the value of the quench radius, the radius at which the induction parameter must be evaluated can be determined by comparisons with experiments or calculations performed with a detailed model.

After performing a series of studies which tested and calibrated the similarity model in cylindrical and spherical geometries, the detailed model was reconfigured to evaluate the quench radius and the minimum ignition energy of a particular gas mixture. This study provided insight into the source of the disagreement between the predictions of the similarity and detailed models at very small radii of energy deposition. The error occurred because the definition of an induction time is only valid for a volume of material that is large and homogeneous enough in temperature and pressure so that diffusive effects are not important. In the cases where the radii of deposition were very small, increased thermal conductivity due to a steep temperature gradient eroded the high temperature region too quickly. Thus in the competition between chemical energy release to heat a region and thermal conduction to cool it, thermal conduction dominated.

Further limits of validity of the simplified model should now be tested. These include investigating the sensitivity of predictions to time or mode of energy deposition, to variations in the chemical induction time, and to the effects of radiative losses discussed in the Appendix. These kinds of calibrations and determinations of the limitations and sensitivity of the similarity model are extremely important if we are to establish the level of accuracy required for input data. Once this has been done, the similarity model can be used with experimental input data to estimate quickly whether a material is flammable and if so, how much energy is required to ignite it. Another extension of the work presented here involves using the detailed simulation to investigate the effect of geometry and method of energy deposition on ignition energies and quenching distances. Both these studies are currently being pursued.

ACKNOWLEDGEMENTS

The authors would like to acknowledge the help and encouragement of Drs. T. R. Young and H. Carhart in preparing this work. This research has been sponsored by the Naval Material Command and the Naval Research Laboratory through the Office of Naval Research.

APPENDIX

The derivation of the similarity solution model is discussed in detail here for the case of spherically symmetric geometry. Assuming that the pressure field is essentially constant and that no shocks are present, the conservation equations for momentum and energy may be combined to give

$$\frac{dp}{dt} \approx 0 = -\gamma \underline{P} \underline{v} \cdot \underline{v} + \underline{v} \cdot \lambda N k_B \underline{v} T + S(t) e^{-k^2(t)r^2} \quad (A1)$$

where κ and the Gaussian energy deposition term, $S(t) e^{-k^2 r^2}$, have already been discussed. The other equation required is the continuity equation,

$$\frac{1}{\rho} \frac{dp}{dt} = -\underline{v} \cdot \underline{v} \quad (A2)$$

Assuming $dP/dt \approx 0$, Eq. (A1) gives an algebraic equation for $\underline{v} \cdot \underline{v}$ which may be combined with Eq. (A2) to give

$$\frac{1}{T} \frac{dT}{dt} = \frac{S(t)}{P_\infty \gamma} e^{-k^2(t)r^2} + \underline{v} \cdot \frac{\kappa}{T} \underline{v} T \quad (A3)$$

where P_∞ is the background pressure. The solution is then

$$T(r, t) = T_\infty e^{A(t) e^{-k^2(t)r^2}} \quad (A4)$$

and

$$\rho(r, t) = \rho_\infty e^{-A(t) e^{-k^2(t)r^2}} \quad (A5)$$

where T_∞ and ρ_∞ are the background temperature and density, respectively. Thus the nonlinear slow flow equations including expansions and contractions of the flow have been converted into a single equation which is linear in the logarithm of the temperature.

The total energy of the system at any instant is the sum of the internal energy and the work performed in expanding the heated region. It may be written

$$E(t) = \frac{P_\infty \gamma}{\gamma-1} \int_0^\infty 4\pi r^2 dr \left[1 - \frac{\rho(r, t)}{\rho_\infty} \right] \quad (A6)$$

$$= \frac{\gamma P_\infty}{(\gamma-1)k^3(t)} \int_0^\infty 4\pi x^2 \left[1 - e^{-Ax} \right] dx$$

$$= \frac{\gamma P_\infty}{(\gamma-1)k^3(t)} F(A(t)). \quad (A7)$$

which defines the integral $F(A(t))$. Differentiating this we find that

$$\frac{dE}{dt} = \frac{\pi^{3/2} S(t)}{(\gamma-1)k^3(t)} \quad (A8)$$

which may be equated to

$$\frac{dE}{dt} = \frac{\partial E}{\partial k} \frac{\partial k}{\partial t} + \frac{\partial E}{\partial A} \frac{\partial A}{\partial t}. \quad (A9)$$

Thus a consistency condition has been specified on the rates of change of the amplitude, $A(t)$, and the scale size $k^{-1}(t)$ for the heated region.

If the fluid velocity v is then expanded such that

$$v(r) \approx v_1(t) r, \quad (A10)$$

that is, only the linear term is kept, two coupled ordinary differential equations for k and A may be obtained,

$$\frac{dk}{dt} = -kv_1 - 2\kappa k^3 \quad (A11)$$

$$\frac{dA}{dt} = \frac{S(t)}{\gamma P} - 6\kappa k^2 A. \quad (A12)$$

Then the expression for v_1 may be written in terms of the integral $F(A)$

$$v_1 = \frac{S}{3\gamma P_\infty} \frac{F'(0) - F'(A)}{F(A)} + 2\kappa k^2 \frac{AF'(A) - F(A)}{F(A)} \quad (A13)$$

which results from using the principle of energy conservation and equating Eqs. (A8) and (A9).

EFFECT OF RADIATIVE LOSSES

When a large amount of energy is deposited in a small volume, the effect of radiative losses may be significant. Exact calculation of all the low temperature radiation effects is still beyond even the best detailed calculations today. An idealized model can be included in the similarity solution, however, to estimate these effects.

Black body radiation from a spherical surface at radius r takes energy out of the system at a rate

$$\frac{dE_{rad}}{dt} = 4\pi r^2 \sigma T^4(r). \quad (A14)$$

In the similarity solution the temperature at any radius r is given by

$$T(r, t) = T_\infty e^{A(t)e^{-k^2(t)r^2}}. \quad (A15)$$

Therefore, $\frac{dE_{rad}}{dt} = 4\pi\sigma T_\infty^4 r^2 e^{4A(t)e^{-k^2(t)r^2}}.$ (A16)

However at $t = 0$ ($A = 0$),

$$\frac{dE_{rad}}{dt} = 0. \quad (A17)$$

Therefore the background radiation into the volume must be subtracted from (A 16) to give

$$\frac{dE_{rad}}{dt} = 4\pi\sigma T_\infty^4 r^2 e^{4A(t)e^{-k^2(t)r^2}} - 4\pi\sigma T_\infty^4 r^2. \quad (A18)$$

The next step is to choose r such that Eq. A18 is maximized. By assuming that the loss from the system proceeds at the maximum rate possible, the model is sure to signal the onset of radiative loss effects at least as soon as they occur in the physical system itself.

REFERENCES

1. Oran, E. S., and Boris, J. P., Prog. Energy Combustion Science. 7:1-72 (1981).
2. Oran, E. S., and Boris, J. P., presented at the 7th International Colloquium on Gas Dynamics of Explosions and Reactive Systems, Göttingen, 1979.
3. Lewis, B., and von Elbe, G., Combustion, Flames and Explosions of Gases, Academic Press, New York, San Francisco, London, 1961, pp. 323-367.
4. Weinberg, F. J., and Wilson, J. R., Proc. R. Soc. Lond. A321, 41-52 (1971).
5. Kingdon, R. G., and Weinberg, F. J., Sixteenth Symposium (International) on Combustion, The Combustion Institute, Pittsburgh, 1977, p. 747.
6. Dixon-Lewis, G., and Shepherd, I. G., Fifteenth Symposium (International) on Combustion, The Combustion Institute, Pittsburgh, 1975, p. 1483.
7. Dixon-Lewis, G., Combustion Flame 33, 319-321 (1978).
8. Overley, J. R., Overholser, K. A., and Reddien, G. W., Combustion Flame 31, 69-83 (1978).
9. Ballal, D. R., and Lefebvre, A. H., Proc. R. Soc. Lond. A357, 163-181 (1977).
10. Williams, F. A., Combustion Theory, Addison Wesley, Reading, Palo Alto, London, 1965, p. 2.
11. Boris, J. P., ADINC: An Implicit Lagrangian Hydrodynamics Code, N.R.L. Memorandum Report 4022, Naval Research Laboratory, Washington, D.C., 1979.
12. Jones, W. W., and Boris, J. P., Flame - A Slow Flow Combustion Model, N.R.L. Memorandum Report 3790, Naval Research Laboratory, Washington, D.C., 1979.
13. Burks, T. L., and Oran, E. S., A Computational Study of the Chemical Kinetics of Hydrogen Combustion, N.R.L. Memorandum Report 4446, Naval Research Laboratory, Washington, D.C., 1980.
14. Stull, D. R., and Prophet, H., JANAF Thermochemical Tables, National Standard Reference Data Series, U. S. National Bureau of Standards, No. 37, 2nd Ed., Gaithersburg, Maryland, 1971.

15. Young, T. R., and Boris, J. P., J. Phys. Chem. 81, 2424-2427 (1977).
16. Young, T. R., CHEMQ, A Subroutine for Solving Stiff Ordinary Differential Equations, N.R.L. Memorandum Report 4091, Naval Research Laboratory, Washington, D.C., 1980.
17. Jones, W. W., and Boris, J. P., J. Phys. Chem. 81, 2532-2534 (1977).
18. Oran, E. S., Boris, J. P., Young, T. R., Flanigan, M., Burks, T., and Picone, M., Eighteenth Symposium (International) on Combustion, The Combustion Institute, Pittsburgh, 1981.
19. Mason, E. A., and Saxena, S.C., Phys. Fluids 1, 361-369 (1958).
20. Blanc, M. V., Guest, P. G., von Elbe, G., and Lewis, B., J. Chem. Phys. 15, 798-802 (1947).
21. Lewis, B., and von Elbe, G., Combustion, Flame and Explosions of Gases, Academic Press, New York, San Francisco, London, 1961, p. 326.
22. Taki, S., and Fujiwara, T., Proc. AIAA 9th Fluid and Plasma Dynamics Conference, 1-9 (1976).
23. Kailasanath, K., Oran, E.S., Boris, J.P., and Young, T.R., A One-Dimensional Time-Dependent Model For Flame Initiation, Propagation and Quenching, to be published as N.R.L. Memorandum Report, Naval Research Laboratory, Washington, D.C., 1981.
24. Baulch, D.L., Drysdale, D.C., Horne, D.G., and Lloyd, A.C., Evaluated Kinetic Data for High Temperature Reactions, Vol. 1, Butterworths, London, 1972.
25. Hampson, R.F., and Garvin, D., "Chemical Kinetic and Photochemical Data for Modelling of Atmospheric Chemistry," NBS Technical Note 866, National Bureau of Standards, Washington, D.C. (1975).
26. Choen, N., and Westberg, K.R., "Data Sheets," The Aerospace Corporation, P.O. Box 92957, Los Angeles, California (1979).

27. Olson, D.B., and Gardiner, W.C., J. Phy. Chem., 81, 2514 (1977).
28. Lloyd, A.C., Int. J. Chem. Kinetics, 6 169 (1974).
29. Bahn, G.S., "Reaction Rate Compilation for H-O-N System," Gordon and Breach, New York, 1968.

Table I. H_2-O_2 Elementary Reactive Mechanism

Reaction	$k_1 = AT^B \exp(-C/T)$ (a)			Reference
	A (b)	B	C (b)	
$H + HO \rightleftharpoons O + H_2$	1.40(-14) 3.00(-14)	1.00 1.00	3.50(+03) 4.48(+03)	[24] [24]
$H + HO_2 \rightleftharpoons H_2 + O_2$	4.20(-11) 9.10(-11)	0.00 0.00	3.50(+02) 2.91(+04)	[24] [24]
$H + HO_2 \rightleftharpoons HO + HO$	4.20(-10) 2.00(-11)	0.00 0.00	9.50(+02) 2.02(+04)	[24] [24]
$H + HO_2 \rightleftharpoons O + H_2O$	8.30(-11) 1.75(-12)	0.00 0.45	5.00(+02) 2.84(+04)	$k_r = k_f/k_c$ [25]
$H + H_2O_2 \rightleftharpoons HO_2 + H_2$	2.80(-12) 1.20(-12)	0.00 0.00	1.90(+03) 9.40(+03)	[24] [24]
$H + H_2O_2 \rightleftharpoons HO + H_2O$	5.28(-10) 3.99(-10)	0.00 0.00	4.50(+03) 4.05(+04)	$k_r = k_f/k_c$ [24]
$HO + H_2 \rightleftharpoons H + H_2O$	1.83(-15) 1.79(-14)	1.30 1.20	1.84(+03) 9.61(+03)	[26] [26]
$HO + HO \rightleftharpoons H_2 + O_2$	1.09(-13) 2.82(-11)	0.26 0.00	1.47(+04) 2.42(+04)	$k_f = k_r/k_c$ [27]
$HO + HO \rightleftharpoons O + H_2O$	1.00(-16) 3.20(-15)	1.30 1.16	0.00(+00) 8.77(+03)	$k_r = k_f/k_c$ [26]
$HO + HO_2 \rightleftharpoons H_2O + O_2$	8.30(-11) 2.38(-10)	0.00 0.17	5.03(+02) 3.69(+04)	$k_r = k_f/k_c$ [28]
$HO + H_2O \rightleftharpoons HO_2 + H_2$	1.70(-11) 4.70(-11)	0.00 0.00	9.10(+02) 1.65(+04)	[24] [24]
$HO + O_3 \rightleftharpoons HO_2 + O_2$	1.60(-12) 6.69(-14)	0.00 0.33	9.56(+02) 2.04(+04)	$k_r = k_f/k_c$ [25]
$HO + H_2 \rightleftharpoons HO + H_2O$	1.20(-12) 1.33(-14)	0.00 0.43	9.41(+03) 3.62(+04)	$k_r = k_f/k_c$ [27]
$HO_2 + HO_2 \rightleftharpoons H_2O_2 + O_2$	3.00(-11) 1.57(-09)	0.00 -0.38	5.00(+02) 2.20(+04)	$k_r = k_f/k_c$ [25]

Table I. (continued)
 $\text{H}_2\text{-O}_2$ Elementary Reactive Mechanism

Reaction	$k_1 = AT^B \exp(-C/T)$ ^(a)			Reference
	A ^(b)	B	C ^(b)	
$\text{O} + \text{HO} \rightleftharpoons \text{H} + \text{O}_2$	2.72(-12) 3.70(-10)	0.28 0.00	-8.10(+01) 8.45(+03)	$k_f = k_r / K_c$ [24]
$\text{O} + \text{HO}_2 \rightleftharpoons \text{HO} + \text{O}_2$	8.32(-11) 2.20(-11)	0.00 0.18	5.03(+02) 2.82(+04)	$k_r = k_f / K_c$ [28]
$\text{O} + \text{H}_2\text{O}_2 \rightleftharpoons \text{H}_2\text{O} + \text{O}_2$	1.40(-12) 5.70(-14)	0.00 0.52	2.12(+03) 4.48(+04)	$k_r = k_f / K_c$ [25]
$\text{O} + \text{H}_2\text{O}_2 \rightleftharpoons \text{HO} + \text{HO}_2$	1.40(-12) 2.07(-15)	0.00 0.64	2.13(+03) 8.23(+03)	$k_r = k_f / K_c$ [25]
$\text{H} + \text{H} + \text{M} \rightleftharpoons \text{H}_2 + \text{M}$	1.80(-30) 3.70(-10)	-1.00 0.00	0.00(+00) 4.83(-04)	[24] [24]
$\text{H} + \text{HO} + \text{M} \rightleftharpoons \text{H}_2\text{O} + \text{M}$	6.20(-26) 5.80(-09)	-2.00 0.00	0.00(+00) 5.29(+04)	[24] [24]
$\text{H} + \text{O}_2 + \text{M} \rightleftharpoons \text{HO}_2 + \text{M}$	4.14(-33) 3.50(-09)	0.00 0.00	-5.00(+02) 2.30(+04)	[24] [24]
$\text{HO} + \text{HO} + \text{M} \rightleftharpoons \text{H}_2\text{O}_2 + \text{M}$	2.50(-33) 2.00(-07)	0.00 0.00	-2.55(+03) 2.29(+04)	[24] [24]
$\text{O} + \text{H} + \text{M} \rightleftharpoons \text{HO} + \text{M}$	8.28(-29) 2.33(-10)	-1.00 0.21	0.00(+00) 5.10(+04)	$k_r = k_f / K_c$ [29]
$\text{O} + \text{HO} + \text{M} \rightleftharpoons \text{HO}_2 + \text{M}$	2.80(-31) 1.10(-04)	0.00 -0.43	0.00(+00) 3.22(+04)	$k_r = k_f / K_c$ [29]
$\text{O} + \text{O} + \text{M} \rightleftharpoons \text{O}_2 + \text{M}$	5.20(-35) 3.00(-06)	0.00 -1.00	-9.00(+02) 5.94(+04)	[24] [24]

(a) Bimolecular reaction rate constants are given in units of $\text{cm}^3/(\text{molecule sec})$.
 Termolecular reaction rate constants are given in units of $\text{cm}^6/(\text{molecule}^2 \text{ sec})$.

(b) Exponentials to the base 10 are given in parenthesis; i.e., $1.00(-10) = 1.00 \times 10^{-10}$.

Table II

Case	Initial Radius of Deposition R_0 (cm)	Total Energy Deposited E_0 (mJ)	<u>Ignition Prediction</u>	
			Detailed Numerical Simulation	Similarity Solution
1	0.1	4.0	yes	yes
		3.7	yes	yes
		3.0	no	no
2	0.11	5.0	yes	yes
		3.0	no	no
3	0.12	7.0	yes	yes
		6.0	no	no
4	0.09	3.3	no	yes
5	0.08	3.3	no	yes

FIGURE CAPTIONS

Figure 1 Time history of the temperature profile in a $H_2:O_2:N_2/2:1:10$ mixture as predicted by the detailed numerical simulation model.

Figure 2 Temperature as a function of induction time for $H_2:O_2:N_2/2:1:10$ mixture evaluated using the chemical reaction scheme in Table I.

Figure 3 The nonlinear amplitude, A , and the characteristic radius, R_c , as functions of time calculated using the similarity solution model.

Figure 4 Calculations of the central temperature as a function of time for three values of E_0 using the detailed numerical simulation model.

Figure 5 The central temperature as a function of time for three values of E_0 as predicted by the similarity solution model.

Figure 6 Calculations of the induction parameter as a function of time for three values of E_0 using the similarity solution model. The "*" indicates the predicted time of ignition.

Figure 7 Comparisons of the time history of the temperature profiles predicted by the detailed numerical model and the similarity solution model.

Figure 8 The minimum ignition energy as a function of the radius of energy deposition calculated using detailed numerical simulations.

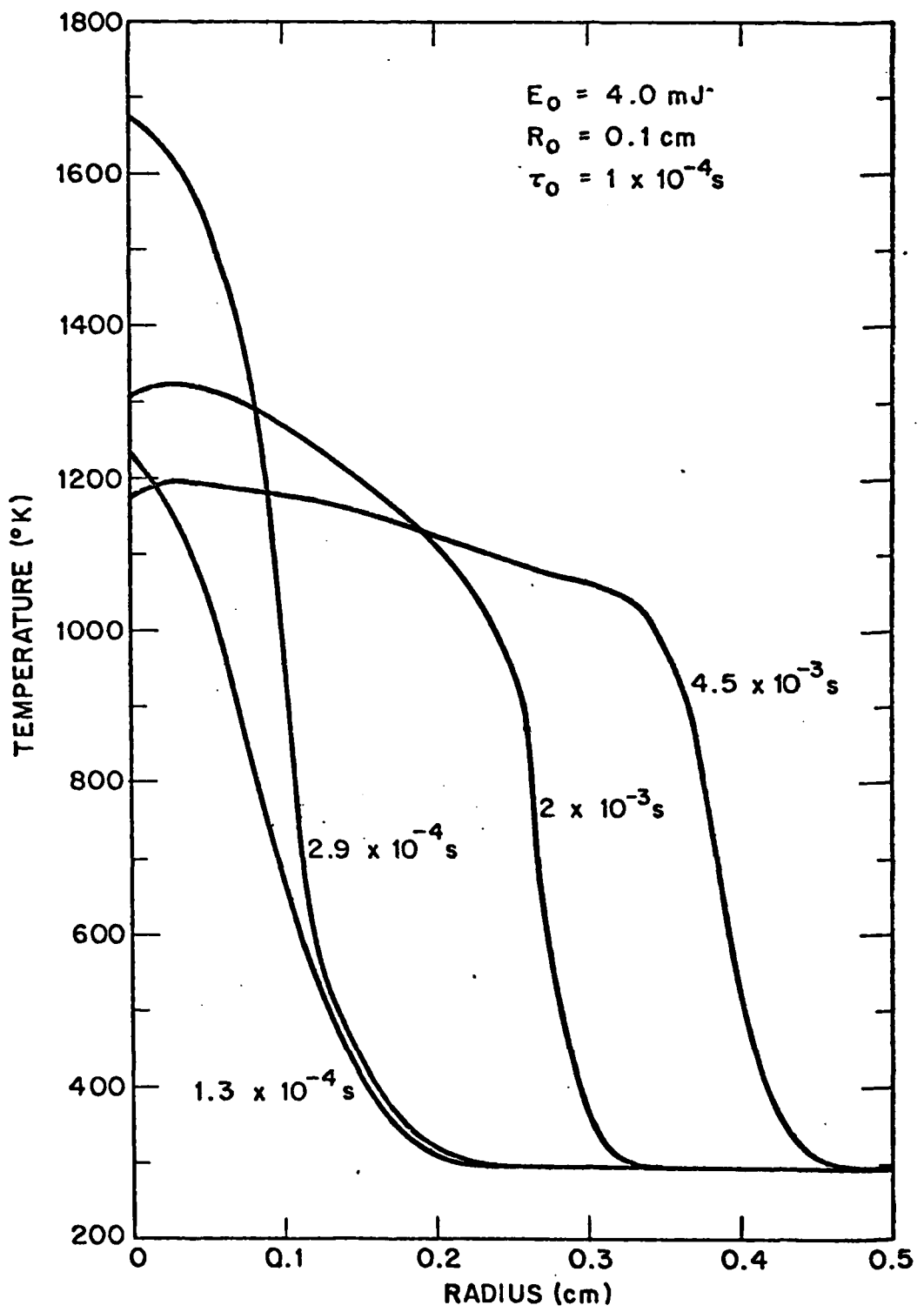


Figure 1

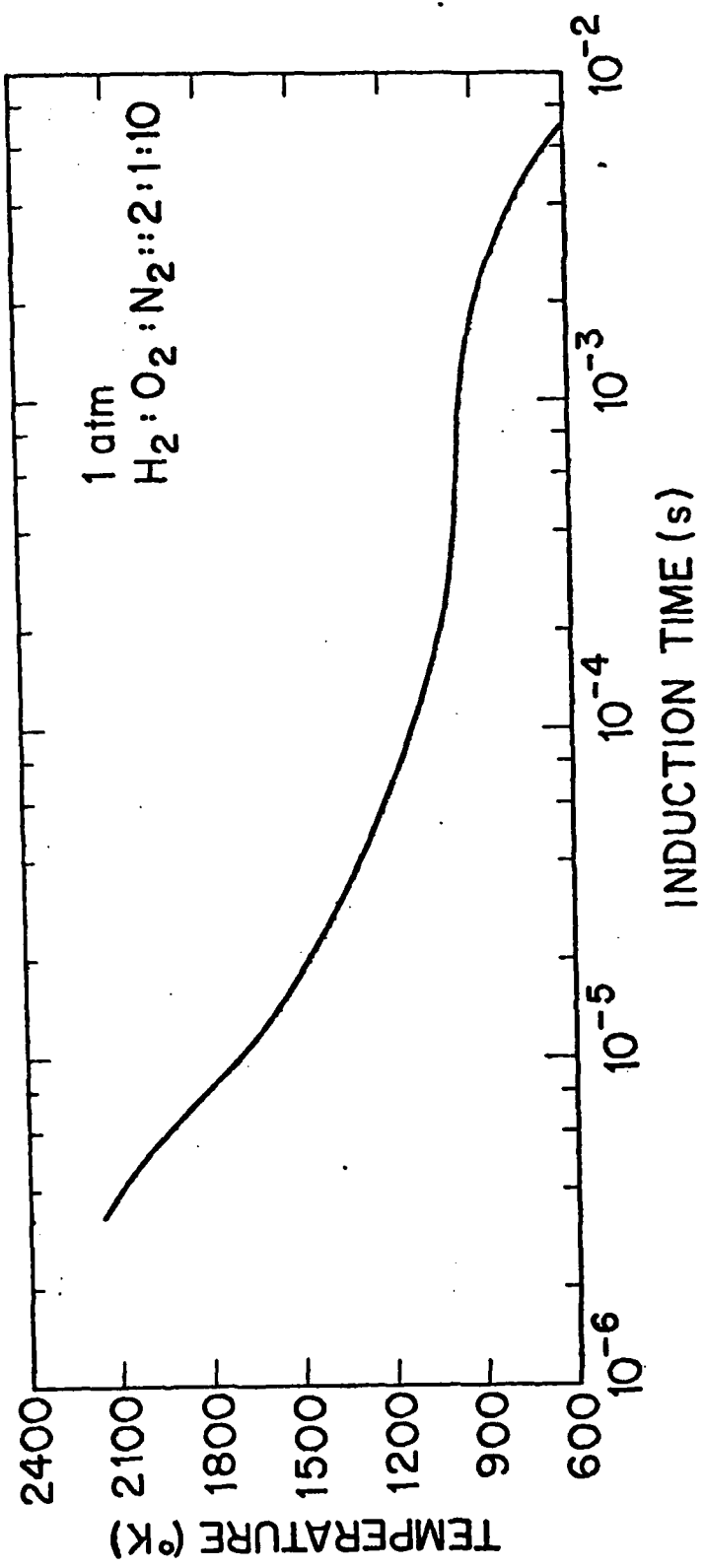


Figure 2

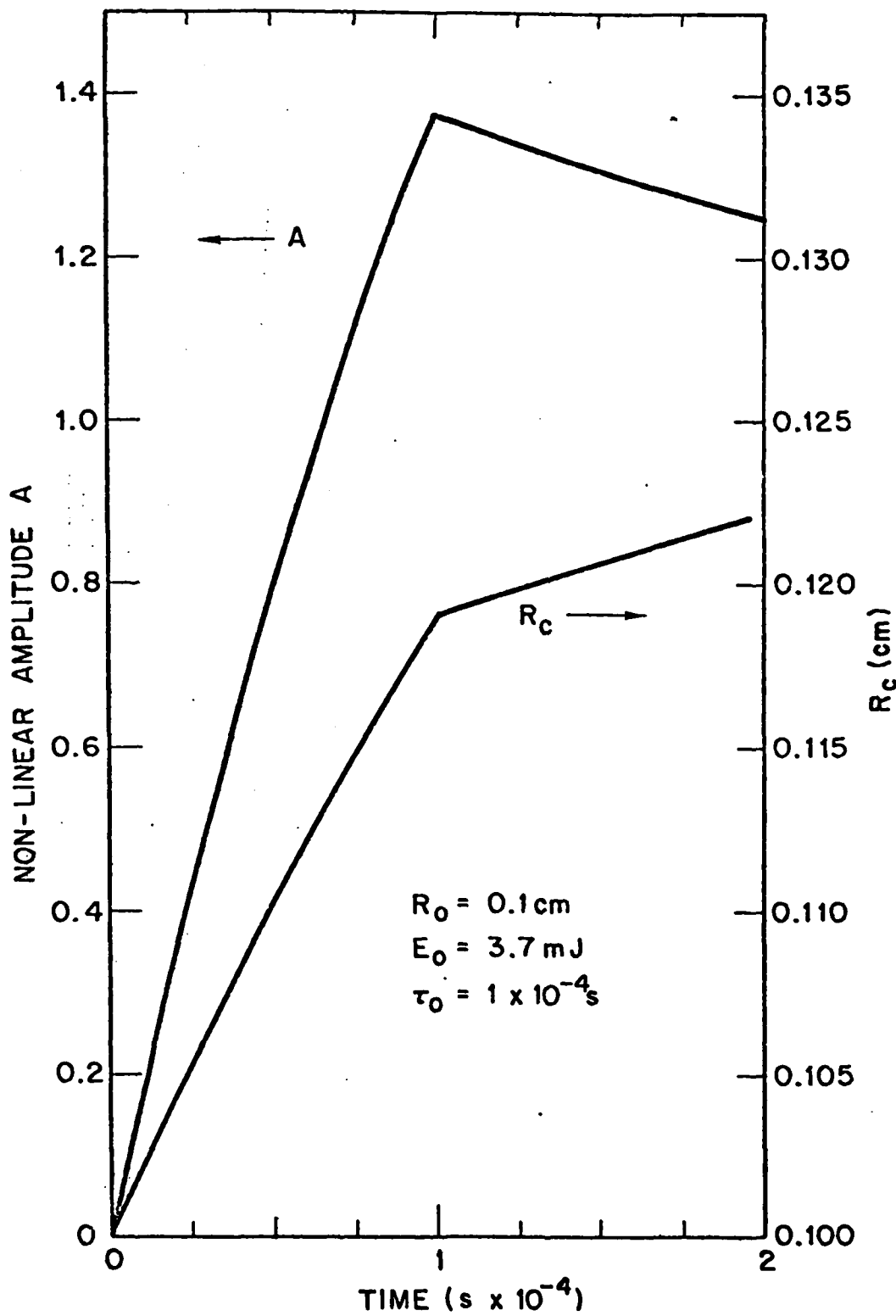


Figure 3

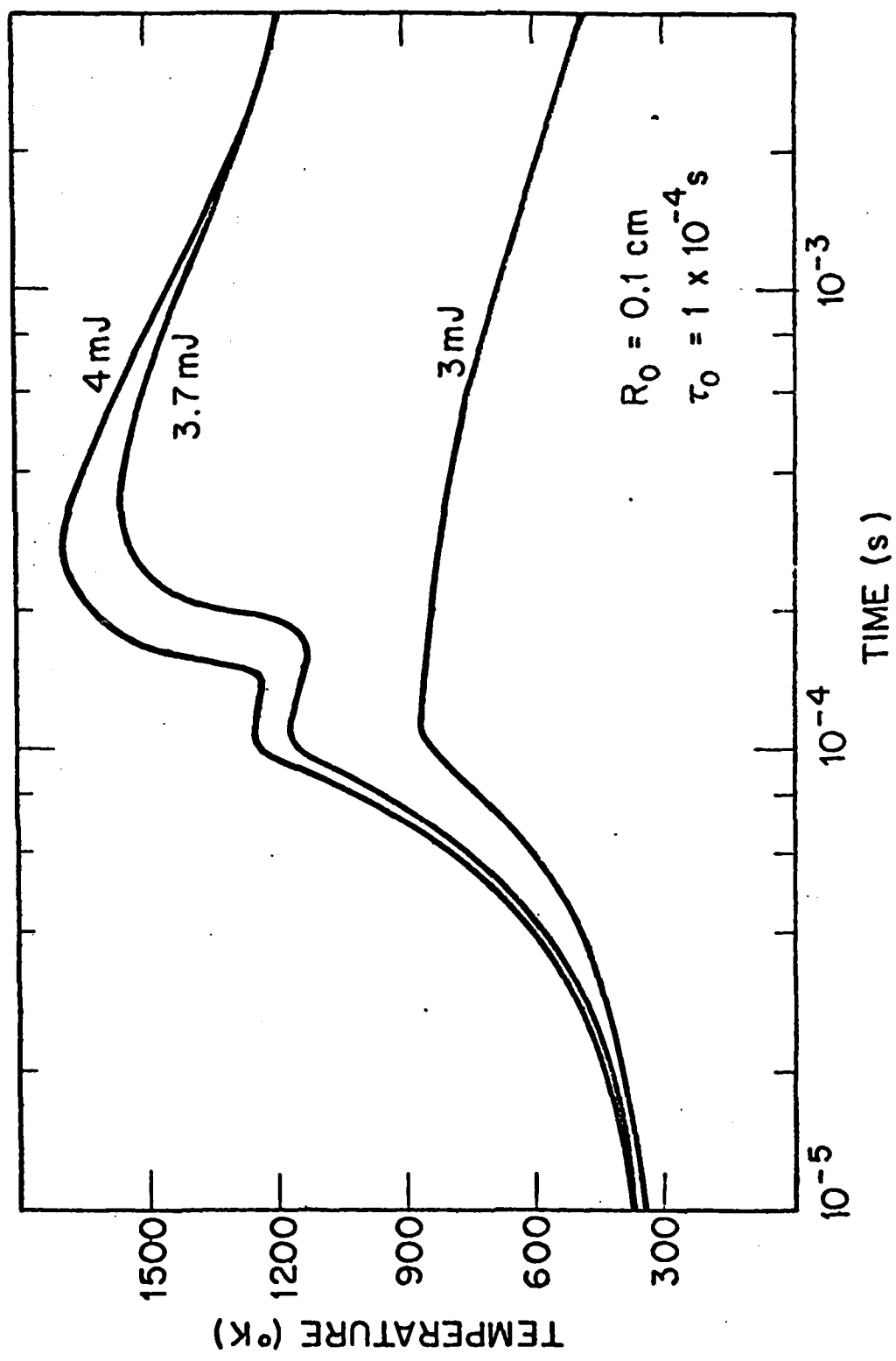


Figure 4

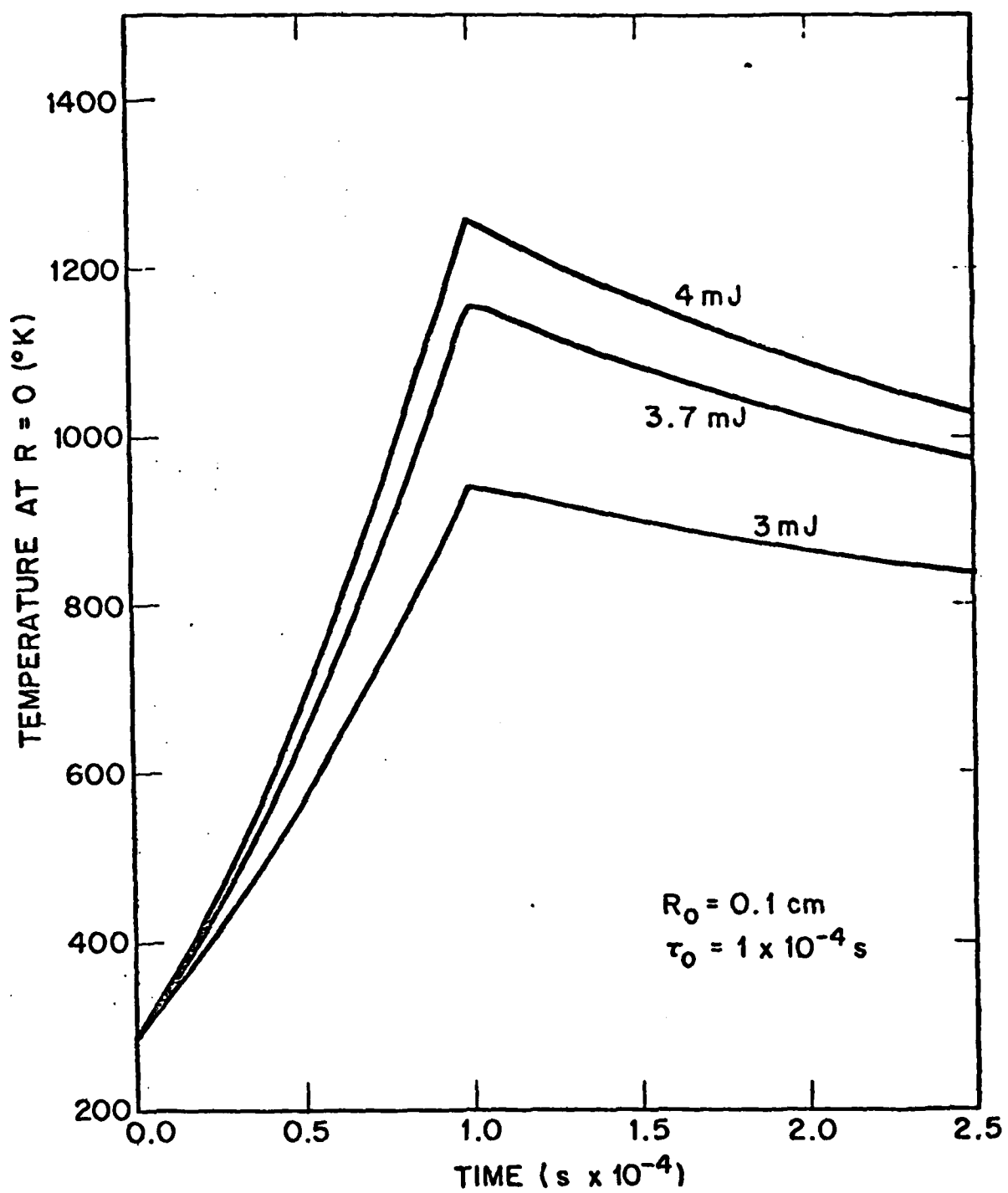


Figure 5

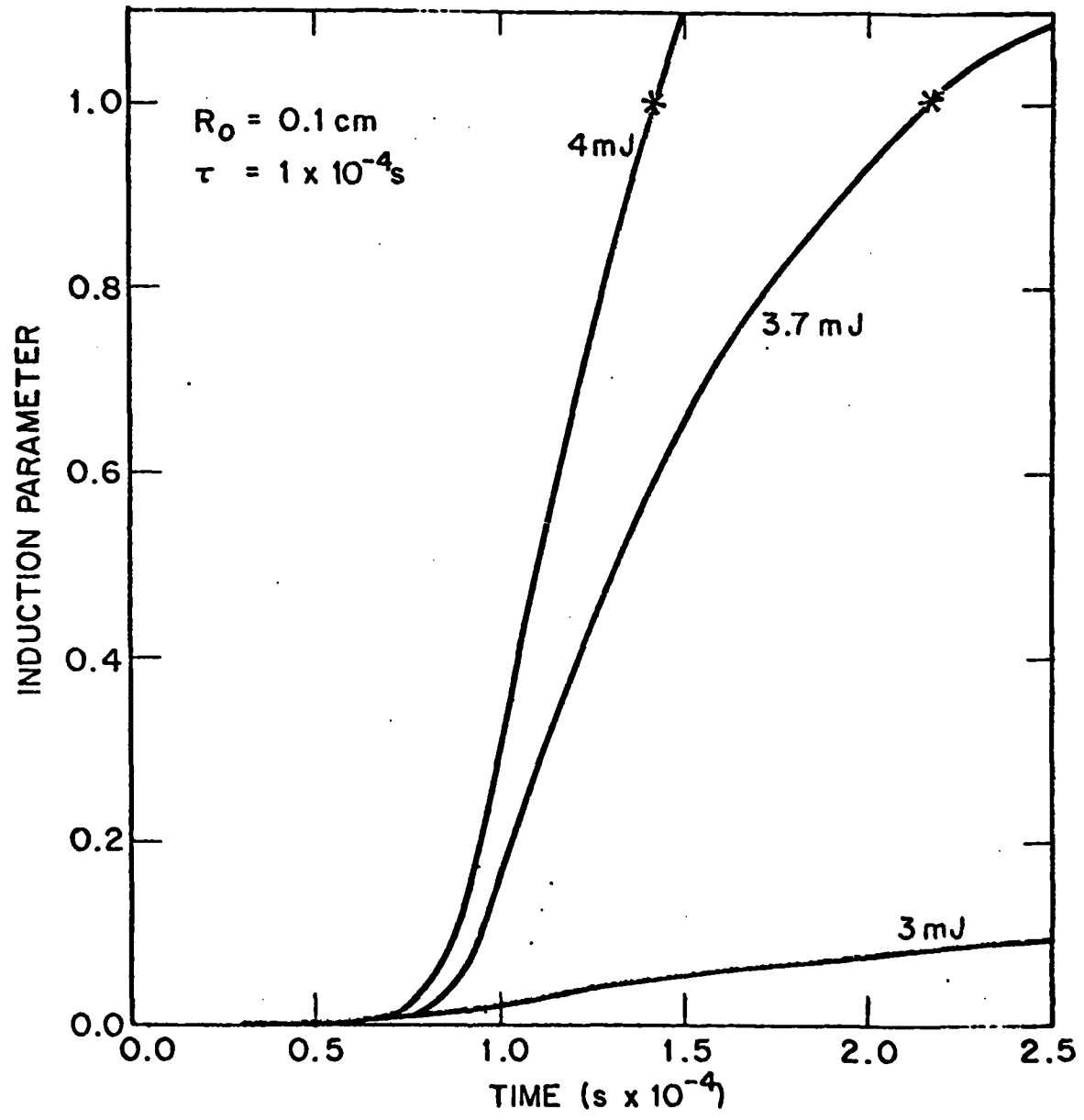


Figure 6

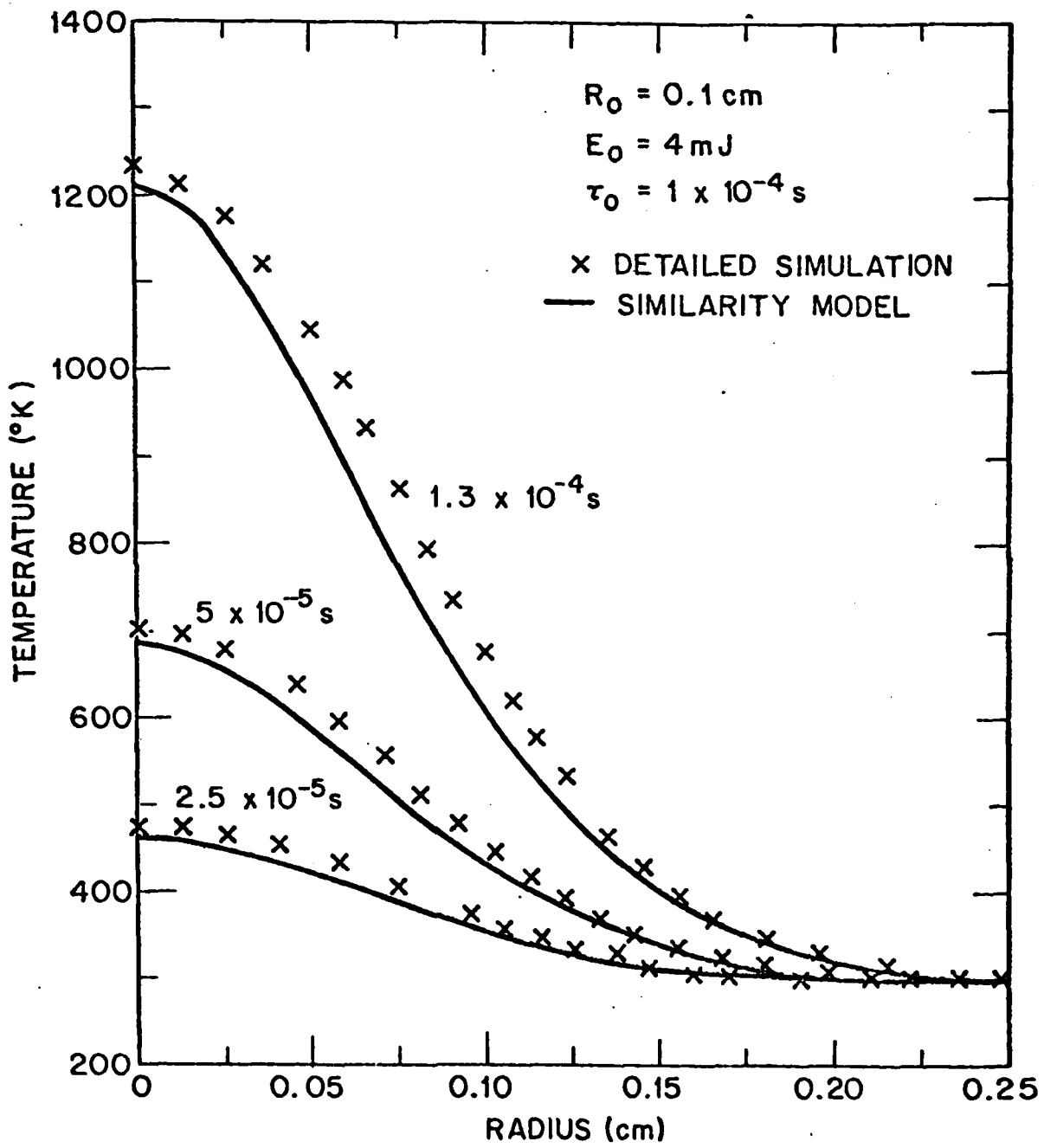


Figure 7

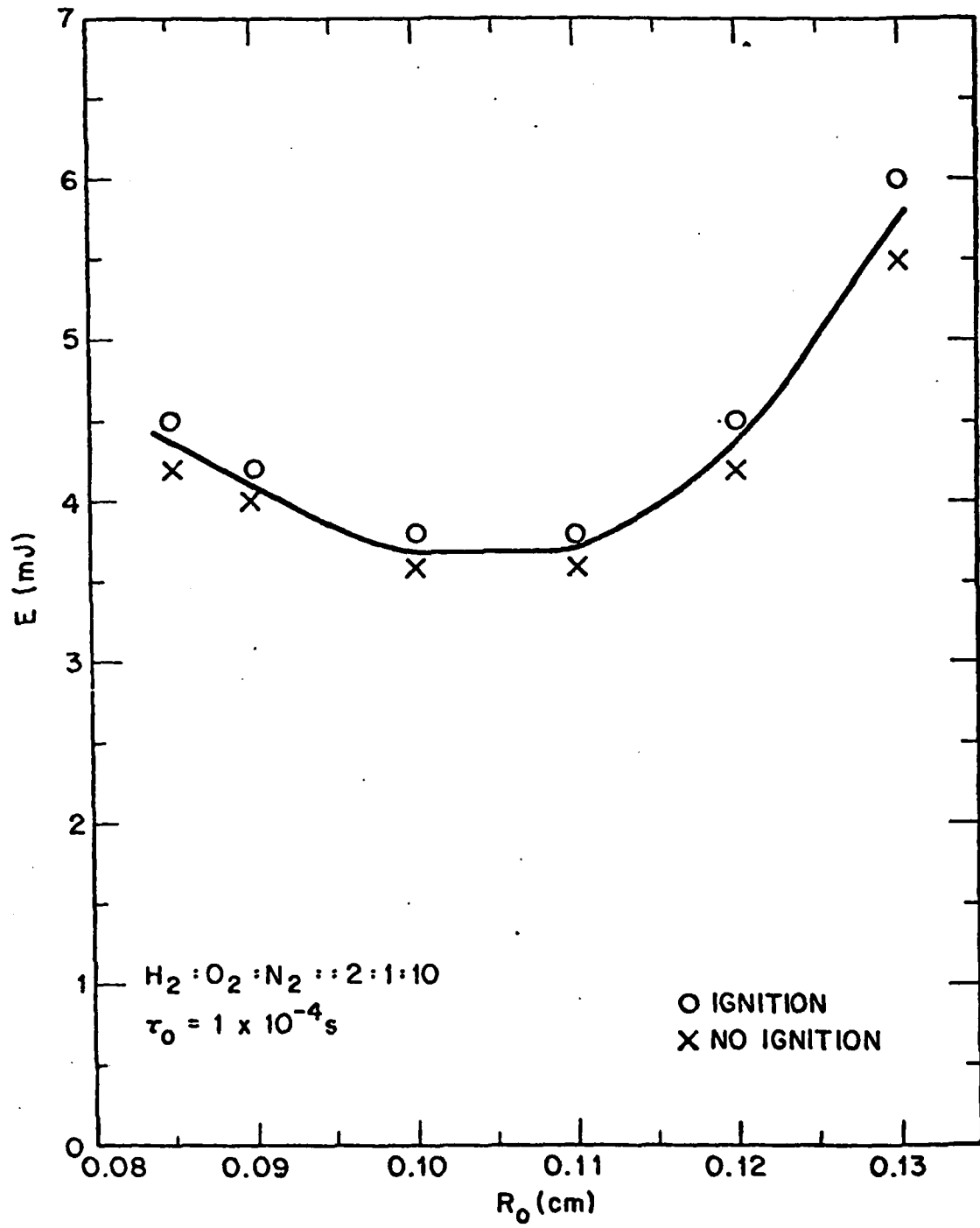


Figure 8

Appendix C
REVISED SUBROUTINES - INITIAL AND RTCON

CIFER -- VERSION 06.05

DATE = 12/08/81 TIME = 10121152197

PAGE 5

*** MEDIUM INITIAL ***

OLD MDT = 01.342

TIME = 101211

CHECKSUM = 27011800

501 C MAXSTP
502 C MAX
503 C MAX
504 C MAX

JAXI

1

1A1

1

1A2

1

1A3

1

1A4

1

1A5

1

1A6

1

1A7

1

1A8

1

1A9

1

1A10

1

1A11

1

1A12

1

1A13

1

1A14

1

1A15

1

1A16

1

1A17

1

1A18

1

1A19

1

1A20

1

1A21

1

1A22

1

1A23

1

1A24

1

1A25

1

1A26

1

1A27

1

1A28

1

1A29

1

1A30

1

1A31

1

1A32

1

1A33

1

1A34

1

1A35

1

1A36

1

1A37

1

1A38

1

1A39

1

1A40

1

1A41

1

1A42

1

1A43

1

1A44

1

1A45

1

1A46

1

1A47

1

1A48

1

1A49

1

1A50

1

1A51

1

1A52

1

1A53

1

1A54

1

1A55

1

1A56

1

1A57

1

1A58

1

1A59

1

1A60

1

1A61

1

1A62

1

1A63

1

1A64

1

1A65

1

1A66

1

1A67

1

1A68

1

1A69

1

1A70

1

1A71

1

1A72

1

1A73

1

1A74

1

1A75

1

1A76

1

1A77

1

1A78

1

1A79

1

1A80

1

1A81

1

1A82

1

1A83

1

1A84

1

1A85

1

1A86

1

1A87

1

1A88

1

1A89

1

1A90

1

1A91

1

1A92

1

1A93

1

1A94

1

1A95

1

1A96

1

1A97

1

1A98

1

1A99

1

1A100

1

1A101

1

1A102

1

1A103

1

1A104

1

1A105

1

1A106

1

1A107

1

1A108

1

1A109

1

1A110

1

1A111

1

1A112

1

1A113

1

1A114

1

1A115

1

1A116

1

1A117

1

1A118

1

1A119

1

1A120

1

1A121

1

1A122

1

1A123

1

1A124

1

1A125

1

1A126

1

1A127

1

1A128

1

1A129

1

1A130

1

1A131

1

1A132

1

1A133

1

1A134

1

1A135

1

1A136

1

1A137

1

1A138

1

1A139

1

1A140

1

1A141

1

1A142

1

1A143

1

1A144

1

1A145

1

1A146

1

1A147

1

CIFER -- VFRSIGN 06.03

DATE = 12/08/81 TIME = 101211 CHECKSUM = 2F00100A

*** MEMRFF INITIAL

PLT DATA = 81.342 TIME = 101211

PAGE 4

101 C 16 - 17 THE TYPE OF BOUNDARY CONDITION FOR THE
102 C CONTINUITY (QUATION) TO USE AT THE HIGH
103 C ALTITUDE (13)
104 C 18 - 25 THE HIGH ALTITUDE AT WHICH THE BOUNDARY
105 C CONDITION IS APPLIED (FB.1)
106 C 26 - 33 FOR MINOR NEUTRALS, THE BOUNDARY VALUE (FB.1)
107 C 34 - 41 FOR MINOR NEUTRALS, A DIFFUSION COEFFICIENT
108 C (FB.1)
109 C 42 - 44 HANLY
110 C 45 A ONE CHARACTER SYMBOL TO USE ON PLT'S TO
111 C IDENTIFY THIS SECTION (A1)

112 C THE LAST CARD IN THIS SECTION GIVES THE ORDER IN WHICH
113 C THE CONTINUITY EQUATIONS ARE TO BE SOLVED WITH ALL THE
114 C IONS DONE BEFORE ANY MINOR NEUTRAL
115 C
116 C

5) INITIAL PROFILES

117 C FOR EACH ALTITUDE AT WHICH INITIAL CONDITIONS ARE KNOWN
118 C THREE (3) CARDS ARE USED
119 C THE FIRST CARD GIVES THE ALTITUDE (22), THE TWO
120 C COMPONENTS OF THE NEUTRAL KINCS (U,V), AND
121 C THE VIBRATIONAL ENERGY OF H2 (EV9). (FB.1)
122 C THE SECOND CARD GIVES THE ION DENSITIES (BX,TEO.1)
123 C THE THIRD CARD GIVES THE MINOR NEUTRAL DENSITIES
124 C (PX,TCO.1)

6) PRINT CONTROL VARIABLES IN TWO NAMELISTS IN SURROUNTING DISPLAY

NAMELIST "PRINT"

125 C L11 A LOGICAL VARIABLE, TRUE IF THE
126 C HYDRODYNAMIC VARIABLES ARE TO BE PRINTED
127 C 137 C 140 C 141 C 142 C 143 C 144 C 145 C 146 C 147 C 148 C 149 C 150 C 151 C
138 C 139 C 141 C 142 C 143 C 144 C 145 C 146 C 147 C 148 C 149 C 150 C 151 C
139 C 140 C 141 C 142 C 143 C 144 C 145 C 146 C 147 C 148 C 149 C 150 C 151 C
140 C 141 C 142 C 143 C 144 C 145 C 146 C 147 C 148 C 149 C 150 C 151 C
141 C 142 C 143 C 144 C 145 C 146 C 147 C 148 C 149 C 150 C 151 C
142 C 143 C 144 C 145 C 146 C 147 C 148 C 149 C 150 C 151 C
143 C 144 C 145 C 146 C 147 C 148 C 149 C 150 C 151 C
144 C 145 C 146 C 147 C 148 C 149 C 150 C 151 C
145 C 146 C 147 C 148 C 149 C 150 C 151 C
146 C 147 C 148 C 149 C 150 C 151 C
147 C 148 C 149 C 150 C 151 C
148 C 149 C 150 C 151 C
149 C 150 C 151 C
150 C 151 C

CIFER -- VERSION 66.03

DATE = 12/08/81 TIME = 10:342

PAGE 5

DATE = 12/08/81 TIME = 10:342

PAGE 5

152. C DEFAULT, *FALSE*.
153. C A LOGICAL VARIABLE, *TRUE*, IF PLOTS OF
154. C SELECTED DENSITIES VS ALTITUDE ARE TO BE
155. C MADE -- DEFAULT, *FALSE*.
156. C THE MINIMUM AND MAXIMUM ALTITUDE COVERED
157. C IN THE PLOTS -- DEFAULT, 106.0, 500.0.
158. C A LOGICAL VARIABLE, *TRUE*, IF LOGGING
159. C PLOTS ARE DESIRED.
160. C THE HOUR, DAY AND INCREMENT IN ALTITUDE
161. C INDEX AT WHICH TO PRODUCE PINCHED OUTPUT
162. C FOR USE AS INITIAL CONDITIONS.
163. C SELECTED HOURS OF THE DAY AT WHICH
164. C PRINTED OUTPUT IS DESIRED.
165. C THE INCREMENT IN THE ALTITUDE INDEX FOR
166. C PRINTED OUTPUT.
167. C THE NUMBER OF HOURS BETWEEN PRINTED OUTPUT
168. C IS THE HOUR OF THE DAY THAT PRINTED OUTPUT
169. C IS TO START.
170. C THE DAY THAT PRINTED OUTPUT IS TO START
171. C A LOGICAL VARIABLE, *TRUE*, IF PRINTED
172. C OUTPUT IS TO BE GENERATED AFTER EVERY STEP.
173. C -- DEFAULT, *FALSE*.
174. C THE FIRST THREE ARE NOT CURRENTLY USED. THEY ARE ASSOCIATED
175. C WITH TAKING PLOTS TO FILM WHICH HAS NOT BEEN IMPLEMENTED.
176. C
177. C
178. C
179. C
180. C
181. C
182. C
183. C
184. C
185. C
186. C
187. C
188. C
189. C
190. C
191. C
192. C
193. C
194. C
195. C
196. C
197. C
198. C
199. C
200. C
201. C
202. C
NAMELIST "RASTER".
NAMELIST VARIABLES FOR PLOTS TO FILM NOT CURRENTLY USED.
PASXL
PASXR
PASXT
PASXTL
PASXTN
PASXO
PASYI
XRNBL
XRNBL
XRNBL
XRNBL
SRC
WRT
IGT

7 CIRCUITRY HARMONIC PATTS ART

CIEP -- VERSION 06.03

DATE = 12/08/81

TIME = 10124

CHCKSUM = 27801B88

PAGE 6

** MEMOIPR INITIAL

2034 C SFT "RTCON" FOR DESCRIPTION OF INPUT CARDS.

2044 C 8) INITIALIZE DEPOSITION ROUTINES

2054 C THROUGH SUBROUTINE REINIT

2064 C

2074 C

2084 C

2094 C

2104 C

2114 C

2124 C

2134 C

2144 C

2154 C

2164 C

2174 C

2184 C

2194 C

2204 C

2214 C

2224 C

2234 C

2244 C

2254 C

2264 C

2274 C

2284 C

2294 C

2304 C

2314 C

2324 C

2334 C

2344 C

2354 C

2364 C

2374 C

2384 C

2394 C

2404 C

2414 C

2424 C

2434 C

2444 C

2454 C

2464 C

2474 C

2484 C

2494 C

2504 C

2514 C

2524 C

2534 C

1. A"LIST "TALPRT"

VARIABLES USED TO MAKE A DEPOSITION TABLE, IF DESIRED.

LSPT THE UNIT NUMBER OF THE FILE CONTAINING OR
TO CONTAIN THE TABLE (SLE "MONTLH")

INPT A TABLE IDENTIFIED -- DEFAULT 0

DEFAUTL GIVES NO TABLE. SFT "MONTLH")

MATT THE JACCHIA MODEL TO USE FOR COMPUTING THE

THE DEPOSITION TABLE

HRSTIN THE MINIMUM HOUR IN THE TABLE --

HRSTAX THE MAXIMUM HOUR IN THE TABLE --

HRST THE NUMBER OF TIME INTERVALS FOR THE TABLE

-- DEFAULT 96

ALTRIN THE MINIMUM ALTITUDE IN THE TABLE --

ALTRAX THE MAXIMUM ALTITUDE IN THE TABLE --

ALTR DEFAULT 2 STOP

ALTRTS THE NUMBER OF ALTITUDE INTERVALS IN THE

TABLE -- DEFAULT 112-1

HRTR(2) THE TYPE OF GRID SPACING FOR THE TABLE.

DEFAULT 0, 1

THIS SECTION ALSO READS THE VARIOUS CROSS SECTION

FOR THE DAYTIME AND NIGHTTIME POSITION

THE PROGRAM SIZE ***

THE RAPORT TRNS

THE MAXIMUM NUMBER OF GRID POINTS

RACTIV THE MAXIMUM NUMBER OF ACTIVE SPECIES

(TRANS PLUS MIND MINTERALS)

MATRS THE MAXIMUM NUMBER OF SPECIES

(not counting fractions)

HR THE MAXIMUM INPUT OF CROSSE SECTION

CLIBP == VERSION 06.03

DATE = 12/00/81

PAGE: 7

REC#	REPORT INITIAL	REC DATE = 01.34?	REC = 10124	CHECKSUM = 2741186
2540	C			(INCLUDING REPOSITION)
2554	C	PRP	THE MAXIMUM NUMBER OF REACTIONS INVOLVING DEPOSITION	
2564	C	PRP	THE MAXIMUM NUMBER OF REACTANTS PER REACTION	
2574	C			
2584	C			
2594	C			
2600	C	THE VARIABLES:		
2614	C	PR	THE ACTUAL NUMBER OF GRID POINTS USED	
2624	C			
2634	C	ICNS	THE ACTUAL NUMBER OF IONS	
2644	C			
2654	C	INSP1	INNS + 1	
2664	C			
2674	C	INSPS	THE ACTUAL NUMBER OF MINOR NEUTRAL SPECIES	
2684	C			
2694	C	INNS	INNS + MINERS	
2704	C			
2714	C	INSP1	INNS + 1	
2724	C			
2734	C	INSPS	THE ACTUAL NUMBER OF MAJOR NEUTRAL SPECIES	
2744	C			
2754	C	INATNS	INNS + MAJORS	
2764	C			
2774	C	INATNP1	INATNS + 1	
2784	C			
2794	C	IPR	THE ACTUAL NUMBER OF CHEMICAL REACTIONS	
2804	C			(INCLUDING REPOSITION)
2814	C			
2824	C	IPR	THE ACTUAL NUMBER OF REACTIONS INVOLVING DEPOSITION	
2834	C			
2844	C	IPR	THE ACTUAL MAXIMUM NUMBER OF REACTANTS PER REACTION	
2854	C			
2864	C	PARANTTP	H2 = 151	
2874	C	PARANTTP	NaClIV = 14	
2884	C	PARANTTP	NaOH = 14	
2894	C	PARANTTP	NaOHs = 2n	
2904	C	PARANTTP	NaOHs = INATNS + 1	
2914	C	PARANTTP	NaR = 70	
2924	C	PARANTTP	NaR = 25	
2934	C	PARANTTP	NaR = 3	
2944	C			
2954	C	COMPL: / SIZE / H2, INNS, INSP1, INSPS, IATNS, IATNP1, MAJORS,		
2964	C			
2974	C			
2984	C	THE VARIABLES AND VARIABLS OTHER ASSOCIATED JTER'S	***	
2994	C			
3004	C	THE C-13/S13 VARIABLES		
3014	C			
3024	C	A SIX CHARACTER SYMBOL TO INDICATE EACH SPECIE		
3034	C			
3044	C	CLUDING FILTERINGS		

SIEBEL - VERSIÓN 6.6.61

0011 - 13/00/001

TIME = 10:30:52

MEMPHIS INITIAL FILE DATE = 01-3-92 TIME = 18124 ENTRCKWIR = 258711880

3C5a	C	THE ATOMIC MASS OF EACH SPECIE
3C5b	C	THE ATOMIC SPECIES DENSITIES
3C5c	C	THE ELECTRON DENSITY AT THE OLD AND NEW TIME STEP
3C5d	C	THE MINIMUM VALUE THAT A DENSITY CAN HAVE
3C5e	C	AT A GRID POINT
3C5f	C	AN INDEX GIVING THE TYPE OF BOUNDARY CONDITION
3C5g	C	TO APPLY
3C5h	C	THE LOCATION OF THE UPPER BOUNDARY FOR EACH SPECIE
3C5i	C	FOR THE PURPOSES OF THE CONTINUITY EQUATION
3C5j	C	FOR THE MINOR NEUTRALS, A BOUNDARY VALUE
3C5k	C	FOR THE MINOR NEUTRALS, A DIFFUSION COEFFICIENT
3C5l	C	THE ORDER IN WHICH THE VARIOUS CONTINUITY EQUATIONS
3C5m	C	ARE SOLVED -- ALL ION EQUATIONS MUST BE SOLVED
3C5n	C	BEFORE ANY MINOR NEUTRAL EQUATION
3C5o	C	ASYNTHL (6, "ATMPL1), IN ("ACTIV1), RNSCP ("ACTIV1)
3C5p	C	ASP ("HZ, "ATMPLS), AN ("ACTIV1), RNSP ("HZ
3C5q	C	UR ("ACTIV1), AV ("ACTIV1), AT ("ACTIV1)
3C5r	C	RCRTRR / CVAR / ASYML, AM, ASP, RE, DMNL, LH, HI, BV, MA,
3C5s	C	PARTRR
3C5t	C	THE HYDROGENATOMIC VARIABLES
3C5u	C	THE AMBIENT MAJOR NEUTRAL TEMPERATURE
3C5v	C	THE ION TEMPERATURE AT THE OLD AND NEW TIME STEP
3C5w	C	THE ELECTRON TEMPERATURE AT THE OLD AND NEW TIME STEP
3C5x	C	THE MINOR NEUTRAL WIND VELOCITY IN THE X- DIRECTION
3C5y	C	THE MINOR NEUTRAL WIND VELOCITY IN THE Y- DIRECTION
3C5z	C	THE VIBRATIONAL ENERGY AT 1:2 -- NOT CURRENTLY USED
3C5aa	C	RVIP
3C5ab	C	THE PRESSURE GRADIENT IN THE X-DIRECTION
3C5ac	C	THE PRESSURE GRADIENT IN THE Y-DIRECTION
3C5ad	C	LOW FREQUENCY COLLISION FREQUENCY

DATE = 12/08/81 TIME = 1012115219
 DATE = 12/08/81 TIME = 1012115219
 *** MEDIUM INITIAL MEDIUM INITIAL MEDIUM INITIAL
 3564 C RTH VISCOSITY
 3574 C RYRF EDY DIFFRUSION COEFFICIENT
 3584 C RYRF EDY DIFFRUSION COEFFICIENT
 3594 C RYRF EDY DIFFRUSION COEFFICIENT
 3604 C RYRF TN(M2), T1(M2,2), T2(M2,2)
 3614 C RYRF U(M2,2), V(M2,2), EVIN(M2)
 3624 C RYRF DPX(M2), DPY(M2), VIN(M2), WEN(M2),
 3634 C RYRF FDYDE(M2)
 3644 C CPMR(M2) / HVAP / TH, T1, T2, U2, V2, EV1B,
 3654 C CPMR(M2) / HVAP / TH, T1, T2, U2, V2, EV1B,
 3664 C CPMR(M2) / HVAP / TH, T1, T2, U2, V2, EV1B,
 3674 C CPMR(M2) / HVAP / TH, T1, T2, U2, V2, EV1B
 3684 C CPMR(M2) / HVAP / TH, T1, T2, U2, V2, EV1B
 3694 C CPMR(M2) / HVAP / TH, T1, T2, U2, V2, EV1B
 3704 C RTH THE SECOND INDEX FOR ASP WHERE H
 3714 C RTH THE SECOND INDEX FOR ASP WHERE H
 3724 C RTH THE SECOND INDEX FOR ASP WHERE H
 3734 C RTH THE SECOND INDEX FOR ASP WHERE H
 3744 C RTH THE SECOND INDEX FOR ASP WHERE H
 3754 C RTH THE SECOND INDEX FOR ASP WHERE H
 3764 C RTH THE SECOND INDEX FOR ASP WHERE H
 3774 C RTH THE SECOND INDEX FOR ASP WHERE H
 3784 C RTH THE SECOND INDEX FOR ASP WHERE H
 3794 C RTH THE SECOND INDEX FOR ASP WHERE H
 3804 C RTH, RTH, RTH, RTH, RTH, RTH, RTH
 3814 C RTH, RTH, RTH, RTH, RTH, RTH, RTH
 3824 C RTH, RTH, RTH, RTH, RTH, RTH, RTH
 3834 C RTH, RTH, RTH, RTH, RTH, RTH, RTH
 3844 C RTH, RTH, RTH, RTH, RTH, RTH, RTH
 3854 C RTH, RTH, RTH, RTH, RTH, RTH, RTH
 3864 C RTH, RTH, RTH, RTH, RTH, RTH, RTH
 3874 C THE VARIANTS
 3884 C Z THE GRID POINTS --- ALTITUDE (IN KM)
 3894 C Z THE GRID POINTS --- ALTITUDE (IN KM)
 3904 C CPOZ INFORMATION: ANNUAL GRID SPACING
 3914 C CPOZ INFORMATION: ANNUAL GRID SPACING
 3924 C RSC P=0.2, WHERE P IS THE RADIAL GEODETIC DISTANCE
 3934 C RSC RSC
 3944 C RSC RSC
 3954 C RSC RSC
 3964 C RSC RSC
 3974 C Z(M2), E(M2), RRSN(M2), RSD(M2)
 3984 C Z(M2), E(M2), RRSN(M2), RSD(M2)
 3994 C CPMR(M2) / Z, RRDZ, PRSD, RSD
 4004 C CPMR(M2) / Z, RRDZ, PRSD, RSD
 4014 C THE SCALAR VARIABLE(S)
 4024 C U2(M2)
 4034 C U2(M2)
 4044 C U2(M2)
 4054 C U2(M2)
 4064 C U2(M2)

INITIAL	NAME	DEFINITION	UNITS
007.	R21		
008.	R22		
009.	R23		
010.	R24		
011.	R25		
012.	R26		
013.	R27		
014.	R28		
015.	R29		
016.	R30		
017.	R31		
018.	R32		
019.	R33		
020.	R34		
021.	R35		
022.	R36		
023.	R37		
024.	R38		
025.	R39		
026.	R40		
027.	R41		
028.	R42		
029.	R43		
030.	R44		
031.	R45		
032.	R46		
033.	R47		
034.	R48		
035.	R49		
036.	R50		
037.	R51		
038.	R52		
039.	R53		
040.	R54		
041.	R55		
042.	R56		
043.	R57		
044.	R58		
045.	R59		
046.	R60		
047.	R61		
048.	R62		
049.	R63		
050.	R64		
051.	R65		
052.	R66		
053.	R67		
054.	R68		
055.	R69		
056.	R70		
057.	R71		
058.	R72		
059.	R73		
060.	R74		
061.	R75		
062.	R76		
063.	R77		
064.	R78		
065.	R79		
066.	R80		
067.	R81		
068.	R82		
069.	R83		
070.	R84		
071.	R85		
072.	R86		
073.	R87		
074.	R88		
075.	R89		
076.	R90		
077.	R91		
078.	R92		
079.	R93		
080.	R94		
081.	R95		
082.	R96		
083.	R97		
084.	R98		
085.	R99		
086.	R100		
087.	R101		
088.	R102		
089.	R103		
090.	R104		
091.	R105		
092.	R106		
093.	R107		
094.	R108		
095.	R109		
096.	R110		
097.	R111		
098.	R112		
099.	R113		
100.	R114		
101.	R115		
102.	R116		
103.	R117		
104.	R118		
105.	R119		
106.	R120		
107.	R121		
108.	R122		
109.	R123		
110.	R124		
111.	R125		
112.	R126		
113.	R127		
114.	R128		
115.	R129		
116.	R130		
117.	R131		
118.	R132		
119.	R133		
120.	R134		
121.	R135		
122.	R136		
123.	R137		
124.	R138		
125.	R139		
126.	R140		
127.	R141		
128.	R142		
129.	R143		
130.	R144		
131.	R145		
132.	R146		
133.	R147		
134.	R148		
135.	R149		
136.	R150		
137.	R151		
138.	R152		
139.	R153		
140.	R154		
141.	R155		
142.	R156		
143.	R157		
144.	R158		
145.	R159		
146.	R160		
147.	R161		
148.	R162		
149.	R163		
150.	R164		
151.	R165		
152.	R166		
153.	R167		
154.	R168		
155.	R169		
156.	R170		
157.	R171		
158.	R172		
159.	R173		
160.	R174		
161.	R175		
162.	R176		
163.	R177		
164.	R178		
165.	R179		
166.	R180		
167.	R181		
168.	R182		
169.	R183		
170.	R184		
171.	R185		
172.	R186		
173.	R187		
174.	R188		
175.	R189		
176.	R190		
177.	R191		
178.	R192		
179.	R193		
180.	R194		
181.	R195		
182.	R196		
183.	R197		
184.	R198		
185.	R199		
186.	R200		
187.	R201		
188.	R202		
189.	R203		
190.	R204		
191.	R205		
192.	R206		
193.	R207		
194.	R208		
195.	R209		
196.	R210		
197.	R211		
198.	R212		
199.	R213		
200.	R214		
201.	R215		
202.	R216		
203.	R217		
204.	R218		
205.	R219		
206.	R220		
207.	R221		
208.	R222		
209.	R223		
210.	R224		
211.	R225		
212.	R226		
213.	R227		
214.	R228		
215.	R229		
216.	R230		
217.	R231		
218.	R232		
219.	R233		
220.	R234		
221.	R235		
222.	R236		
223.	R237		
224.	R238		
225.	R239		
226.	R240		
227.	R241		
228.	R242		
229.	R243		
230.	R244		
231.	R245		
232.	R246		
233.	R247		
234.	R248		
235.	R249		
236.	R250		
237.	R251		
238.	R252		
239.	R253		
240.	R254		
241.	R255		
242.	R256		
243.	R257		
244.	R258		
245.	R259		
246.	R260		
247.	R261		
248.	R262		
249.	R263		
250.	R264		
251.	R265		
252.	R266		
253.	R267		
254.	R268		
255.	R269		
256.	R270		
257.	R271		
258.	R272		
259.	R273		
260.	R274		
261.	R275		
262.	R276		
263.	R277		
264.	R278		
265.	R279		
266.	R280		
267.	R281		
268.	R282		
269.	R283		
270.	R284		
271.	R285		
272.	R286		
273.	R287		
274.	R288		
275.	R289		
276.	R290		
277.	R291		
278.	R292		
279.	R293		
280.	R294		
281.	R295		
282.	R296		
283.	R297		
284.	R298		
285.	R299		
286.	R300		
287.	R301		
288.	R302		
289.	R303		
290.	R304		
291.	R305		
292.	R306		
293.	R307		
294.	R308		
295.	R309		
296.	R310		
297.	R311		
298.	R312		
299.	R313		
300.	R314		
301.	R315		
302.	R316		
303.	R317		
304.	R318		
305.	R319		
306.	R320		
307.	R321		
308.	R322		
309.	R323		
310.	R324		
311.	R325		
312.	R326		
313.	R327		
314.	R328		
315.	R329		
316.	R330		
317.	R331		
318.	R332		
319.	R333		
320.	R334		
321.	R335		
322.	R336		
323.	R337		
324.	R338		
325.	R339		
326.	R340		
327.	R341		
328.	R342		
329.	R343		
330.	R344		
331.	R345		
332.	R346		
333.	R347		
334.	R348		
335.	R349		
336.	R350		
337.	R351		
338.	R352		
339.	R353		
340.	R354		
341.	R355		
342.	R356		
343.	R357		
344.	R358		
345.	R359		
346.	R360		
347.	R361		
348.	R362		
349.	R363		
350.	R364		
351.	R365		
352.	R366		
353.	R367		
354.	R368		
355.	R369		
356.	R370		
357.	R371		
358.	R372		
359.	R373		
360.	R374		
361.	R375		
362.	R376		
363.	R377		
364.	R378		
365.	R379		
366.	R380		
367.	R381		
368.	R382		
369.	R383		
370.	R384		
371.	R385		
372.	R386		
373.	R387		
374.	R388		
375.	R389		
376.	R390		
377.	R391		
378.	R392		
379.	R393		
380.	R394		
381.	R395		
382.	R396		
383.	R397		
384.	R398		
385.	R399		
386.	R400		
387.	R401		
388.	R402		
389.	R403		
390.	R404		
391.	R405		
392.	R406		
393.	R407		
394.	R408		
395.	R409		
396.	R410		
397.	R411		
398.	R412		
399.	R413		
400.	R414		
401.	R415		
402.	R416		
403.	R417		
404.	R418		
405.	R419		
406.	R420		
407.	R421		
408.	R422		
409.	R423		
410.	R424		
411.	R425		
412.	R426		
413.	R427		
414.	R428		
415.	R429		
416.	R430		
417.	R431		
418.	R432		
419.	R433		
420.	R434		
421.	R435		
422.	R436		
423.	R437		
424.	R438		
425.	R439		
426.	R440		
427.	R441		
428.	R442		
429.	R443		
430.	R444		
431.	R445		
432.	R446		
433.	R447		
434.	R448		
435.	R449		
436.	R450		
437.	R451		
438.	R452		
439.	R453		
440.	R454		
441.	R455		

CLIFFORD = VERSION OF 03

DATE 12/08/01

11115 3 10921152197

11

LINE NUMBER	INITIAL	FINAL	TIME = 101.342	TIME = 1012.11	CHICKSUNG = 2744111000
1564	C	C1174	CNS(DIPAS)		
1574	C	SRPA1	STH(DIPAS)		
1614	C				
1624	C	CPR			
1634	C	FR1100	HUNDRED OF RADIAN'S PFR DEGREE (PI/180)		
1654	C				
1664	C	CRP1000 / CRP100 / CRP10 / CRP1 / CRP / CRP0	LAT, CLAT, SLAT, DEC, SDEC, SDEC0, RND, CRPA, SRPA, CRPA0, SRPA0, CRPA100, SRPA100		
1674	C				
1684	C				
1694	C				
1704	C				
1714	C				
1724	C				
1734	C				
1744	C				
1754	C				
1764	C				
1774	C				
1784	C				
1794	C				
1804	C				
1814	C				
1824	C				
1834	C				
1844	C				
1854	C				
1864	C				
1874	C				
1884	C				
1894	C				
1904	C				
1914	C				
1924	C				
1934	C				
1944	C				
1954	C				
1964	C				
1974	C				
1984	C				
1994	C				
2004	C				
2014	C				
2024	C				
2034	C				
2044	C				
2054	C				
2064	C				

```

CFLR -- VERSION 06.03
*** MEMBER INITIAL
      509a 4
      510a C
      511a C
      512a C*** PRINTS FOR THE 0+(PC) REACTIONS
      513a C
      514a C 1FOR2R THE REACTION WHOSE CHI-FISTY RATE COEFFICIENT IS 1
      515a C
      516a C 1FOR2R THE NUMBER OF N+(2D) REACTIONS
      517a C 1FOR2R 1FOR2R(J) GIVES THE J-TH FOR2D REACTION
      518a C 1FOR2R 1FOR2D(J) GIVES THE N+1ST REACTANT (OTHER THAN 0+(2D) )
      519a C
      520a C
      521a C
      522a C
      523a C 1FOR2R 1FOR2D(MP), 1FOR2D(MP)
      524a C 1FOR2R / 0FOR2R / LFOR2D, 1FOR2D, 1FOR2D
      525a C
      526a C
      527a C
      528a C
      529a C*** PRINTS FOR PRINTING ***

530a C 1FP THE NUMBER OF PRODUCTION/LOSS TERMS TO PRINT
531a C
532a C
533a C 1FP ALL INTEGER ARRAY GIVING THE INDEX OF EACH
      534a C PRODUCTION/LOSS TERM TO PRINT
      535a C
      536a C 1FOR2R 1FOR2R(MR)
      537a C 1FOR2R / 0FOR2R / 0FOR2R, 1FOR2R
      538a C
      539a C
      540a C
      541a C
      542a C*** SURFACE FOR THE PERIODICITY RATES ***
      543a C
      544a C THE VARIANTS:
      545a C
      546a C 1FP THE PROPRIETION RATES AT THE GRID POINTS
      547a C
      548a C SCR THE TOTAL FOR PRODUCTION RATE
      549a C SCR THE ELECTRON HEATING RATE
      550a C
      551a C
      552a C
      553a C 1FOR2R 1FOR2D(MP)
      554a C 1FOR2R / 0FOR2R / 1FOR2D, SCR, SCR
      555a C
      556a C
      557a C
      558a C
      559a C

```

CIFER -- VERSION 66.03

DATE = 12/06/81 TIME = 10120 CHECKSUM = 2F9188

PAGE. 13

*** READING INITIAL

5604 C IRCL THE NUMBER OF IONIZATION REACTIONS

5614 C IRDR THE NUMBER OF DISSOCIATION REACTIONS

5634 C IRDR THE NUMBER OF REACTIONS INVOLVING BOTH IONIZATION AND DISSOCIATION

5654 C IRDR THE NUMBER OF REACTIONS INVOLVING PURPLEATES OR PREVIOUS POSITION REACTIONS

5694 C IRNT THE NUMBER OF REACTIONS INVOLVING NIGHT TIME DEPOSITIONS

5704 C IRNT THE NUMBER OF REACTIONS INVOLVING NIGHT TIME DEPOSITIONS

5724 C IRXAY THE NUMBER OF REACTIONS INVOLVED IN XRAY PRODUCTION

5734 C IRX1 THE NUMBER OF IONIZATION INDEX IN THE ARRAY 'DEIRAT'

5754 C IRX1 THE NUMBER OF DISSOCIATION INDEX IN THE ARRAY 'DEIRAT'

5764 C IRX1 THE NUMBER OF POSITION INDEXES FOR DISSOCIATION AND IONIZATION

5774 C IRX1 THE NUMBER OF POSITION INDEXES FOR NIGHT TIME DEPOSITION

5804 C IRXAY THE NUMBER OF REACTIONS FOR THE REACTIONS INVOLVED IN XRAY PRODUCTION OF IONS

5824 C IRX1 THE NUMBER OF POSITION INDEXES FOR NIGHT TIME DEPOSITION

5834 C IRX1 THE NUMBER OF POSITION INDEXES FOR NIGHT TIME DEPOSITION

5844 C IRX1 THE NUMBER OF POSITION INDEXES FOR NIGHT TIME DEPOSITION

5854 C IRX1 THE NUMBER OF POSITION INDEXES FOR NIGHT TIME DEPOSITION

5864 C IRX1 THE NUMBER OF POSITION INDEXES FOR NIGHT TIME DEPOSITION

5874 C IRX1 THE NUMBER OF POSITION INDEXES FOR NIGHT TIME DEPOSITION

5884 C IRX1 THE NUMBER OF POSITION INDEXES FOR NIGHT TIME DEPOSITION

5894 C IRX1 THE NUMBER OF POSITION INDEXES FOR NIGHT TIME DEPOSITION

5904 C IRX1 THE NUMBER OF POSITION INDEXES FOR NIGHT TIME DEPOSITION

5914 C IRX1 THE NUMBER OF POSITION INDEXES FOR NIGHT TIME DEPOSITION

5924 C IRXAY THE NUMBER OF REACTIONS FOR THE REACTIONS INVOLVED IN XRAY PRODUCTION OF IONS

5934 C IRX1 THE NUMBER OF POSITION INDEXES FOR NIGHT TIME DEPOSITION

5944 C IRX1 THE NUMBER OF POSITION INDEXES FOR NIGHT TIME DEPOSITION

5954 C IRX1 THE NUMBER OF POSITION INDEXES FOR NIGHT TIME DEPOSITION

5964 C IRX1 THE NUMBER OF POSITION INDEXES FOR NIGHT TIME DEPOSITION

5974 C IRX1 THE NUMBER OF POSITION INDEXES FOR NIGHT TIME DEPOSITION

5984 C IRX1 THE NUMBER OF POSITION INDEXES FOR NIGHT TIME DEPOSITION

5994 C IRX1 THE NUMBER OF POSITION INDEXES FOR NIGHT TIME DEPOSITION

6004 C IRX1 THE NUMBER OF POSITION INDEXES FOR NIGHT TIME DEPOSITION

6014 C IRX1 THE NUMBER OF POSITION INDEXES FOR NIGHT TIME DEPOSITION

6024 C IRX1 THE NUMBER OF POSITION INDEXES FOR NIGHT TIME DEPOSITION

6034 C IRX1 THE NUMBER OF POSITION INDEXES FOR NIGHT TIME DEPOSITION

6044 C IRX1 THE NUMBER OF POSITION INDEXES FOR NIGHT TIME DEPOSITION

6054 C IRX1 THE NUMBER OF POSITION INDEXES FOR NIGHT TIME DEPOSITION

6064 C IRX1 THE NUMBER OF POSITION INDEXES FOR NIGHT TIME DEPOSITION

6074 C IRX1 THE NUMBER OF POSITION INDEXES FOR NIGHT TIME DEPOSITION

6084 C IRX1 THE NUMBER OF POSITION INDEXES FOR NIGHT TIME DEPOSITION

6094 C IRX1 THE NUMBER OF POSITION INDEXES FOR NIGHT TIME DEPOSITION

6104 C IRX1 THE NUMBER OF POSITION INDEXES FOR NIGHT TIME DEPOSITION

*** THE MAIN CONTROL PARAMETERS ***

6144 C IRX1 THE MAXIMUM NUMBER OF TINY STEPS TO COMPUTE

6154 C IRX1 THE MAXIMUM NUMBER OF TINY STEPS TO COMPUTE

6164 C IRX1 THE MAXIMUM NUMBER OF TINY STEPS TO COMPUTE

6174 C IRX1 THE MAXIMUM NUMBER OF TINY STEPS TO COMPUTE

6184 C IRX1 THE MAXIMUM NUMBER OF TINY STEPS TO COMPUTE

6194 C IRX1 THE MAXIMUM NUMBER OF TINY STEPS TO COMPUTE

6204 C IRX1 THE MAXIMUM NUMBER OF TINY STEPS TO COMPUTE

CIFER -- VERSION 16.03

DATE = 12/07/81 TIME = 1012152197

PAGE 14

*** PENTER INITIAL	OLF DAY	81.342	TRIP. = 10121	CHCKSUM = 21P41088
6110 C	1STEP			THE CURRENT STEP
6120 C	PF			THE CURRENT HOUR
6130 C	IRAY			THE CURRENT DAY
6140 C				
6150 C	TRIP			THE TIME STEP IN HOURS
6160 C				
6170 C	YR			THE YEAR FOR THE APPROPRIATE JACCHIA MODEL OF THE
6180 C				AMBIENT NEUTRAL ATMOSPHERE
6190 C				
6200 C	IAOPT			THE NUMBER OF TIME STEPS BETWEEN CALCULATIONS
6210 C				OF THE AMBIENT NEUTRAL TEMPERATURE
6220 C				AND THE MAJOR NEUTRAL DENSITIES
6230 C				
6240 C	PGSCI			PRESSURE GRADIENT SCALF FACTOR
6250 C	ITER			THE NUMBER OF TIME STEPS BETWEEN CALCULATION OF
6260 C				THE DEPOSITION RATES
6270 C				
6280 C	ICHR			A LOGICAL VARIABLE: *TRUE* IF CHEMISTRY IS ON
6290 C				*FALSE* IF CHEMISTRY IS NOT DONE
6300 C				
6310 C	ITHR			A LOGICAL VARIABLE: *TRUE* IF TRANSPORT IS DONE
6320 C				*FALSE* OTHERWISE
6330 C				
6340 C	ITR			THE NUMBER OF ITERATIONS IT TOOK TO GET THE ION
6350 C				EQUATIONS TO CONVERGE
6360 C				
6370 C	CONVR			A LOGICAL VARIABLE: *TRUE* IF THE IONS CONVERGED
6380 C				*FALSE* IF THEY DID NOT
6390 C				
6400 C	LOGICAL			SCHEM, TRIP, CONVRG
6410 C	SCHEM			CONVRG / MTRPL / MAXSTP, MMAX, HR, ISTEP, HR, IDAY, DPH,
6420 C				HR, ISTEP, HR, IDAY, DPH,
6430 C				HR, ISTEP, HR, IDAY, DPH,
6440 C				HR, ISTEP, HR, IDAY, DPH,
6450 C				HR, ISTEP, HR, IDAY, DPH,
6460 C				HR, ISTEP, HR, IDAY, DPH,
6470 C				HR, ISTEP, HR, IDAY, DPH,
6480 C				HR, ISTEP, HR, IDAY, DPH,
6490 C				HR, ISTEP, HR, IDAY, DPH,
6500 C				HR, ISTEP, HR, IDAY, DPH,
6510 C				HR, ISTEP, HR, IDAY, DPH,
6520 C				HR, ISTEP, HR, IDAY, DPH,
6530 C	***			THE QUITUP CONTROL VARIABLES ***
6540 C				
6550 C	THE			QUITUP CONTROL VARIABLES
6560 C				
6570 C	TRIP			THE VALUE IF INAY WHEN "DISPLAY" WAS LAST CALLED
6580 C				
6590 C	ITR			
6600 C				
6610 C	ITR			THE INAYX OR THE ALTITUDE AT WHICH 2ND-UP POINTS

PAGE 15
 DATE = 12/09/81 TIME = 10:24:52.97
 CIEF -- VERSION 06.03
 *** MIEPHEF INITIAL FILE FATT = 81.342 TIME = 101211 CHECKSUM = 27041800
 6621 C ARE TO BE MADE
 6630 C
 6640 C SFRAY THE NUMBER OF SECONDS PER DAY
 6650 C
 6660 C PSY'N1 AN' ARRAY OF SYMBOLS TO IDENTIFY A SPECIE AN THF
 6670 C
 6680 C URNSITY RLET
 6690 C FT AL &? PSY'N1("ATH'P1)
 6700 C
 6710 C CPH'N1 / PCTRL / INFLAY, INTP, SPRAY, NZPLT, PSMBL
 6720 C
 6730 C CPH'N1 / DCTPL / DCIMP, TDIMP, TDIMP, TDIMP
 6740 C THE PR START CONTROL VARIABLES:
 6750 C
 6760 C LFRP
 6770 C
 6780 C LTD'R
 6790 C
 6800 C FRH'R
 6810 C
 6820 C TRU'R
 6830 C IT FRCPR DRIMP, TCIMP
 6840 C
 6850 C CPH'N1 / DCTPL / DCIMP, LTDIMP, LTDIMP, TDIMP
 6860 C
 6870 C
 6880 C
 6890 C *** PRIMER DECLARATIONS ***
 6900 C
 6910 C LPRIC, NSTART
 6920 C IT TIGRP, PLANK
 6930 C MGCPA,MP
 6940 C FTAL &4
 6950 C
 6960 C THIS CIEF'N1 BLANK IS USED BY "DISPLAY" AND "RSTART"!
 6970 C CPH'N1 / START / CPLT / INPT, FZ(121,5)
 6980 C
 6990 C THIS CIEF'N1 PLACE IS USED BY "JACT1"
 7000 C
 7010 C CPH'N1 / START / 75(50), VS(50), EVS(50), ASPS(50, MATHMS)
 7020 C
 7030 C
 7040 C THIS CIEF'N1 PLACE IS USED BY "JACT1"
 7050 C
 7060 C CPH'N1 / INPT / FCN, FCN2, FCN2, EINFD
 7070 C
 7080 C INITIALIZING FIXED CNT.SLSTS ***
 7090 C
 7100 C DATA MATH / 1.011593 / FRAUD / 1.745327 / -02 /
 7110 C DATA PIG / 3.141593 / FRAUD / 1.745327 / -02 /
 7120 C DATA SPRAY / REUNION / SPIN / 3.141593 /

卷之三

RATE = 12/00/81

16

1111 2101 15251697

FILE == VFR1CH66-01

DATE: 12/10/01 TIME: 10:21:02:97

CIFER -- VERSION 06.03

DATE = 12/08/81 TIME = 10124152197

PAGE 19

CHICKEN = CHICKEN

DATE = 12/00/81 VERSN = 06.03 THT = 3103241522497

DATE 8/12/00/81

PAGL. 21

11

C-21

PLAN THE REACTANT PART CONSTANTS ASSOCIATED WITH THE CURRENT
STRUCTURE OF THE "ARROW". ALL THE PREVIOUS REACTIONS MUST BE PLACED AT THE END
OF THE REACTIONS.

THE READING TEST IS AS FOLLOWS

A) THE FIRST SYMBOL IS 'CIRCH' TO INDICATE REACTIONS INVOLVING ENTHALPY

B) THE SECOND SYMBOL IS 'STEPS' TO INDICATE REACTIONS INVOLVING PHOTOREFLECTION

C) FOR MULTI-DEPOSITION REACTIONS THE THIRD SYMBOL IS
 •, FOR IONIZATION
 'E', FOR DISSOCIATION
 'D', FOR IONIZATION AND DISSOCIATION
 'D', FOR A DISSOCIATION OF THE PREVIOUS REACTION

D) THE FOURTH SYMBOL IS 'OPEN' FOR REACTIONS WITH RADICALS AS AN INTERMEDIATE PRODUCT

E) THE FIFTH SYMBOL IS 'INT', TO INDICATE THAT THE DEPOSITION REACTION IS IMPORTANT AT HIGH TIME

F) THE SIXTH SYMBOL IS 'XRAY', FOR THE TWO DEPOSITION REACTIONS INVOLVED IN THE XRAY PRODUCTION OF NO_2 AND NO_3

G) THE SEVENTH SYMBOL IS 'FRINE', IF THE PRODUCTION RATE CONSIDERED IN THIS REACTION IS IN HIGH

2) FOR REACTIONS INVOLVING CHEMISTRY THE NEXT CARD CONTAINS DATA ASSOCIATED WITH THE CHEMICAL REACTION

A) THE FIRST NUMBER IS AN INTEGER GIVING THE APPROPRIATE REACTION LAW

B) THE FIRST THREE NUMBERS ARE THREE CONSTANTS IN THE FORM $\text{NO}_2 \text{NO}_3 \text{NO}_2 \text{NO}_3 \text{NO}_2 \text{NO}_3$ TO CONSTRAIN THE

CIFER -- VERSION 06.03

DATE = 12/07/81

TIME = 10124 CIRCKSUM = 1F220528

PAGE 23

*** MEFRA PIC000011342 TIME = 10124 CIRCKSUM = 1F220528

APPROPRIATE REACTION RATE

520 C	
530 C	
540 C	
550 C	
560 C	*** THE PROGRAM SIZE ***
580 C	
590 C	THE PARAPTRFS1
600 C	**2 THE MAXIMUM NUMBER OF GRID POINTS
610 C	620 C
620 C	**3 THE MAXIMUM NUMBER OF ACTIVE SPECIES
630 C	640 C
640 C	**4 THE MAXIMUM NUMBER (IONS PLUS MINOR NEUTRALS)
650 C	660 C
660 C	**5 THE MAXIMUM NUMBER OF SPECIES
670 C	680 C
680 C	**6 THE MAXIMUM NUMBER OF CHEMICAL REACTIONS
690 C	700 C
700 C	**7 THE MAXIMUM NUMBER (INCLUDING DEPOSITION)
710 C	720 C
720 C	**8 THE MAXIMUM NUMBER OF REACTIONS INVOLVING DEPOSITION
730 C	740 C
740 C	**9 THE MAXIMUM NUMBER OF REACTANTS PER REACTION
750 C	760 C
760 C	**10 THE VARIANTS:
770 C	**12 THE ACTUAL NUMBER OF GRID POINTS USED
780 C	790 C
790 C	**13NS THE ACTUAL NUMBER OF IONS
800 C	810 C
810 C	**14NSPI IONS + 1
820 C	830 C
830 C	**15NS THE ACTUAL NUMBER OF MINOR NEUTRAL SPECIES
840 C	850 C
850 C	**16NS + MINORS
860 C	870 C
870 C	**17NSPI IONS + 1
880 C	890 C
890 C	**18NSPI THE ACTUAL NUMBER OF MAJOR NEUTRAL SPECIES
900 C	910 C
910 C	**19NSPI IONS + MAJORS
920 C	930 C
930 C	**20NSPI IONS + 1
940 C	950 C
950 C	**21NSPI THE ACTUAL NUMBER OF CHEMICAL REACTIONS
960 C	970 C
970 C	**22NSPI (INCLUDING DEPOSITION)
980 C	990 C
990 C	**23NSPI THE ACTUAL NUMBER OF REACTIONS INVOLVING DEPOSITION
1000 C	1010 C
1010 C	**24NSPI THE ACTUAL MAXIMUM NUMBER OF REACTANTS PER REACTION
1020 C	


```

*** PEFPER RICAN      RLC NITR = R1.342    NITC = 10220    CHRCRSUM = 1E220520

154. C    CASE PRINTERS FOR THE N+(2D) REACTIONS
155. C    LRnR2n 11'E REACTION WHOSE CHEMISTRY RATE COEFFICIENT IS 1
156. C    NnRn2n 11'E NUMBER OF N+(2D) REACTIONS
157. C
158. C    ITRnR2n ITRnR2n(J) GIVES THE J=TH OF2D REACTION
159. C
160. C    ITRnR2n ITRnR2n(J) GIVES THE OTHER REACTANT (OTHER THAN N+(2D)) INVOLVED IN THE J=TH OF2D REACTION
161. C
162. C    ITRnR2n ITRnR2n(J) GIVES THE OTHER REACTANT (OTHER THAN N+(2D)) INVOLVED IN THE J=TH OF2D REACTION
163. C
164. C
165. C    ITFRGR ITFRGR(J)N, ITFRGR(J)P
166. C
167. C    ITFRGR / ITFRGR / LRnR2D, NRnR2D, IPRnR2D, IBNnR2D
168. C
169. C
170. C    ITFRGR FOR PRINTING ***

171. C    LRnR 11'E NUMBER OF PRODUCTION/LOSS TFRPS TO PRINT
172. C
173. C    LRnR 11'E NUMBER OF PRODUCTION/LOSS TFRPS TO PRINT
174. C
175. C    ITRP AN INTEGER ARRAY GIVING THE INDEX OF EACH
176. C    PRODUCTION/LOSS TERM TO PRINT
177. C
178. C
179. C    ITTRGR ITTRGR(JN)
180. C    CTRnR / CTRnR / ITRP, ITRP
181. C
182. C
183. C
184. C    SURFACE FOR THE DEPOSITION RATES ***

185. C    THE VARIANTS
186. C
187. C
188. C    ITTRGR 11'E DEPOSITION RATES AT THE GRID POINTS
189. C
190. C    SC1 11'E TOTAL IN: PRODUCTION RATE
191. C    SC1 11'E ELECTRON HEATING RATE
192. C
193. C
194. C
195. C    ITALAN DEPRAT("Z",TRP)
196. C    ITALAN SUR(J2), SUR(J2)
197. C
198. C    CTRnR / CTRnR / ITTRGR, SC1, SC1
199. C
200. C    SC1 PRINTS TO VARIOUS TYPES OF DEPOSITION REACTIONS
201. C
202. C
203. C    ITCS 11'E SURFACE OF INITIALIZATION FUNCTIONS
204. C

```

CIFER - VERSION 06.03

DATE = 12/08/81 TIME = 10121152197

PAGE: 26

```
*** MEMBER RTCON
    205. C  IRTR  THE NUMBER OF DISSOCIATION REACTIONS
    206. C
    207. C  IRTRD  THE NUMBER OF REACTIONS INVOLVING BOTH IONIZATION
    208. C  AND DISSOCIATION
    209. C
    210. C  IRTRD  THE NUMBER OF REACTIONS INVOLVING DUPLICATES OF
    211. C  PREVIOUS REACTION POSITIONS
    212. C
    213. C  IRNT  THE NUMBER OF REACTIONS INVOLVING NIGHT TIME
    214. C  REACTIONS
    215. C
    216. C  IRXRAY  THE NUMBER OF REACTIONS INVOLVED IN XRAY PRODUCTION
    217. C  OF IONS
    218. C  IRTP1  AN INTEGER ARRAY GIVING THE INDEX IN THE ARRAY 'DEPRT'
    219. C  FOR THE IONIZATION RATES
    220. C
    221. C  IRTP2  AN INTEGER ARRAY GIVING THE INDEX IN THE ARRAY 'DEPRT'
    222. C  FOR THE DISSOCIATION RATES
    223. C
    224. C  IRTP3  AN INTEGER ARRAY GIVING THE INDICES FOR DISSOCIATION
    225. C  AND IONIZATION
    226. C
    227. C  IRTP4  AN INTEGER ARRAY GIVING THE INDICES FOR THE
    228. C  DUPLICATES
    229. C
    230. C  IRNT  AN INTEGER ARRAY GIVING THE INDEX FOR NIGHT TIME
    231. C  REACTIONS
    232. C
    233. C  IRTP5  AN INTEGER ARRAY GIVING THE INDICES FOR THE REACTIONS
    234. C  INVOLVED IN XRAY PRODUCTION OF IONS
    235. C
    236. C
    237. C
    238. C  INTCP  INDICES FOR THE REACTIONS
    239. C  INVOLVED IN XRAY PRODUCTION
    240. C
    241. C  COPEN / STROP / IRP1, IRPD, IRP1D, IRP1D, IRXP1, IRXP1D,
    242. C
    243. C
    244. C
    245. C  C444  LOCAL REACTIONS ***
```

246. C
 247. C IRTRP REACTION, SYM1(NCS,ISY), PRH(1), PRH(1)
 248. C IRTRP TEST(2)
 249. C IRTRP TEST(3)
 250. C IRTRP TEST(4)
 251. C IRTRP TEST(5)
 252. C IRTRP TEST(6)
 253. C
 254. C
 255. C

CLIFER -- VERSIÓN 06-03

DATE = 12/08/01 11:11 # 10121152197

```

*** MTRWRF RTCONH      MTR DATA = A1.342  T11'E = 10121  CHCKSUM = 11228528

256*      DATA      REPORT / UTRPO / CHRT / 'CHEM' / 1
257*      DATA      1615Z / J / 1A1D / 11D
258*      DATA      21SSC / J / 1A1D / 11D
259*      DATA      NP201 / J / 1DUP / 11D
259*      DATA      NP202 / J / 1DUP / 11D
260*      DATA      XRAY / J / 11DFT / 11D
261*      DATA      PRINT / PRINI / 1

262*      C***  CHECK FOR FIRST CALL
263*      C***  IF(F1PT .NE. 0) GO TO 50
264*      C***  ICR = 0
265*      C***  IF(I1D .EQ. 0) GO TO 267
266*      C***  ICR = 0
267*      C***  IF(I1D .EQ. 0) GO TO 268
268*      C***  ICR = 0
269*      C***  IF(I1D .EQ. 0) GO TO 270
270*      C***  ICR = 0
271*      C***  IF(F1PT .EQ. 0) GO TO 272
272*      C***  ICR = 0
273*      C***  IF(XRAY .EQ. 0) GO TO 274
274*      C***  ICR = 0
275*      C***  IF(OR20 .EQ. 0) GO TO 276
276*      C***  ICR = 0
277*      C***  IF(PP01 .EQ. 0) GO TO 278
278*      C***  ICR = 0
279*      C***  IF(F1PT .EQ. 0) GO TO 280
280*      C***  PRINT CONTROL LINE FOR THE REACTION
281*      C***  IF(OR20 .EQ. 0) GO TO 282
282*      C***  IF(OR20 .EQ. 0) GO TO 283
283*      C***  PRINT(5,110) (TEST(1),I=1,20)
284*      C***  IF(F1PT .EQ. 0) GO TO 285
285*      C***  IF(F1PT .EQ. 0) GO TO 286
286*      C***  TS THIS REACTION TO BE PRINTED
287*      C***  IF(F1PT .EQ. 0) GO TO 288
288*      C***  IF(F1PT .EQ. 0) GO TO 289
289*      C***  IF(F1PT .EQ. 0) GO TO 290
290*      C***  PRINT(7,110) (PRINT) GO TO 120
291*      C***  PRINT(11,110) (PRINT) GO TO 120
292*      C***  PRINT THIS REACTION INVERSE CHEMISTRY
293*      C***  PRINT(11,110) (PRINT) GO TO 120
294*      C***  PRINT THIS REACTION INVERSE CHEMISTRY
295*      C***  PRINT(11,110) (PRINT) GO TO 200
296*      C***  PRINT(11,110) (PRINT) GO TO 200
297*      C***  A REACTION INVERSE CHEMISTRY
298*      C***  PRINT(11,110) (PRINT) GO TO 120
299*      C***  ICR = ICR + 1
300*      C***  PRINT THE RATIONAL REACTION RATES COEFFICIENTS
301*      C***  PRINT(11,110) (PRINT) GO TO 120
302*      C***  PRINT(11,110) (PRINT) GO TO 120
303*      C***  PRINT(11,110) (PRINT) GO TO 120
304*      C***  PRINT(11,110) (PRINT) GO TO 120
305*      C***  PRINT(11,110) (PRINT) GO TO 120

```

CLUTER = VFRS101, 06.03

DATE = 12/08/81 TINI = 10121 CHECKSUM = 1524528

000 REACTANT RTCAU 010 PART = M1.342 TINI = 10121 CHECKSUM = 1522528

107* Case A REACTION WITHOUT CHIMISTRY (PROPOSITION ONLY)

308* C Part TRANSPORT = 0
310* C Part (PART) = 1.0
311* C Part (PART) = 0.0
312* C Part (PART) = 0.0
313* C Part (PART) = 0.7416.

314* Case A WRITE OUT THE CHIMISTRY RATE COEFFICIENTS

316* C 250 WRITE(6,260)
317* C 260 WRITE(6,260)
318* C 260 WRITE(6,260)
319* C 260 WRITE(6,260)
320* C 260 WRITE(6,260)
321* C 260 WRITE(6,260)
322* C 260 WRITE(6,260)

323* C THIS THE REACTION INVOLVING DEPOSITION

324* C 000 WRITE(6,000)
325* C 000 WRITE(6,000)
326* C 000 WRITE(6,000)
327* C 000 WRITE(6,000)
328* C 000 WRITE(6,000)
329* C 000 WRITE(6,000)

330* C THIS THE REACTION INVOLVING DEPOSITION

331* C 000 WRITE(6,000)

332* C 000 WRITE(6,000)

333* C 000 WRITE(6,000)

334* C 000 WRITE(6,000)

335* C 000 WRITE(6,000)

336* Case A WRITE OUT WHAT KIND OF REACTION IT IS

337* C 000 WRITE(6,000)
338* C 000 WRITE(6,000)
339* C 000 WRITE(6,000)
340* C 000 WRITE(6,000)
341* C 000 WRITE(6,000)

342* Case A WRITE OUT WHAT IF THERE IS AN ERROR

343* C 000 WRITE(6,000)

344* C 000 WRITE(6,000)

345* C 000 WRITE(6,000)

346* C 000 WRITE(6,000)

347* Case A INITITATE

348* C 000 INITIATE

349* C 000 WRITE(6,000)

350* C 000 WRITE(6,000)

351* C 000 WRITE(6,000)

352* C 000 WRITE(6,000)

353* Case A LISSERATION

354* C 000 LISSERATION

355* C 000 LISSERATION

356* C 000 LISSERATION

357* C 000 LISSERATION

CFER -- VERSION 06.03

DATE = 12/08/81

PAGE 29

*** MEMBER REACTN CLR DATA = A1.342 TINF = 10120 CLKSUM = 1E22A52A

3590 C 1590 C 1600 C 1610 C 1620 C 1630 C 1640 C 1650 C 1660 C 1670 C 1680 C 1690 C 1700 C 1710 C 1720 C 1730 C 1740 C 1750 C 1760 C 1770 C 1780 C 1790 C 1800 C 1810 C 1820 C 1830 C 1840 C 1850 C 1860 C 1870 C 1880 C 1890 C 1900 C 1910 C 1920 C 1930 C 1940 C 1950 C 1960 C 1970 C 1980 C 1990 C 2000 C 2010 C 2020 C 2030 C 2040 C 2050 C 2060 C 2070 C

IONIZATION AND DISSOCIATION

IRFID = IRFID + 1
IRID(IRID) = NRD
GP IR SR

IRP1 RATE
IRP1 = IRP1 + 1
IRP1(IRP1) = NRD

IRP2 RATE
IRP2 = IRP2 + 1
IRP2(IRP2) = NRD

CONTINU
IRP3 = TRUE.

LOCATE SPCL' SPECIAL DISPOSITION REACTIONS

CHECK FOR AP20 REACTIONS

IT IS ASSUMED THAT THERE IS ONLY ONE SPECIE REACTING WITH
IRP2 IN THE CURRENT REACTION AND THAT REACTANT IS THE
SPECIE NAMED IN THE REACTION (THE FIRST REACTANT)
IRTEST(1) = IRP2 + 1
IRP2 = IRP2 + 1
IRP2(IRP2) = XRY
IRP2(IRP2) = LPI(2)
IRPLA(IRP1) = EQ. 0 AND. FA(IRP1) = EQ. 1.0) LROP20 = IRP
CONTINU

FINISH THE REACTIONS INVOLVED IN THE NIGHTIME DEPOSITION
IRTEST(5) = EQ. IRP1) = 740
IRP1 = IRP1 + 1
IRP1(IRP1) = NRD
CONTINU
IRTEST(6) = EQ. XRAY + 1
IRXRAY = IRXRAY + 1
IRXRAY(IRXRAY) = 1.0
CONTINU
ERTFID

CHECK FOR XRAY PRODUCTION
IRTEST(1) = IRXRAY + 1
IRXRAY = IRXRAY + 1
IRXRAY(IRXRAY) = 1.0
CONTINU

RTRY MSGN

CFER == VERSION 06.03

DATE = 12/08/81 TIME = 10124 CHECKSUM = 1F226528

PAGE 50

*** MEMBER PICON

0100 C

0101 C

PRINT SPRT ITERS OF INTEREST THAT DID NOT GET PRINTED BY "ARTP"

0102 C

0103 C

0104 C

0105 C

0106 C

0107 C

0108 C

0109 C

0110 C

0111 C

0112 C

0113 C

0114 C

0115 C

0116 C

0117 C

0118 C

0119 C

0120 C

0121 C

0122 C

0123 C

0124 C

0125 C

0126 C

0127 C

0128 C

0129 C

0130 C

0131 C

0132 C

0133 C

0134 C

0135 C

0136 C

0137 C

0138 C

0139 C

0140 C

0141 C

0142 C

0143 C

0144 C

0145 C

0146 C

0147 C

0148 C

0149 C

0150 C

0151 C

0152 C

0153 C

0154 C

0155 C

0156 C

0157 C

0158 C

0159 C

0160 C

0161 C

0162 C

0163 C

0164 C

0165 C

0166 C

0167 C

0168 C

0169 C

0170 C

0171 C

0172 C

0173 C

0174 C

0175 C

0176 C

0177 C

0178 C

0179 C

0180 C

0181 C

0182 C

0183 C

0184 C

0185 C

0186 C

0187 C

0188 C

0189 C

0190 C

0191 C

0192 C

0193 C

0194 C

0195 C

0196 C

0197 C

0198 C

0199 C

0200 C

0201 C

0202 C

0203 C

0204 C

0205 C

0206 C

0207 C

0208 C

0209 C

0210 C

0211 C

0212 C

0213 C

0214 C

0215 C

0216 C

0217 C

0218 C

0219 C

0220 C

0221 C

0222 C

0223 C

0224 C

0225 C

0226 C

0227 C

0228 C

0229 C

0230 C

0231 C

0232 C

0233 C

0234 C

0235 C

0236 C

0237 C

0238 C

0239 C

0240 C

0241 C

0242 C

0243 C

0244 C

0245 C

0246 C

0247 C

0248 C

0249 C

0250 C

0251 C

0252 C

0253 C

*****</p

PAGE 31

DATE = 12/14/81 TIME = 1012452197

CIVER -- VERSION 06.03

*** READER PICON FILE DATE = 81.342 TIME = 10124 CHECKSUM = 1F22A520
1601 SNO1 FORMAT: INSUFFICIENT STORAGE FOR THE POSITION ROUTINE!
1611 1621 STOP
1622 1631 C
1632 RD
1641 *** 464 RECORDS, DATE = 81.342 TIME = 10124 CHECKSUM = 1F22A520
*** READER PICON CAP111

DA
FILM